Available online at www.sciencedirect.com
ScienceDirect
Geochimica et Cosmochimica Acta 72 (2008) 151–169
Geochimica et Cosmochimica Acta
www.elsevier.com/locate/gca

Iron isotopes constrain biologic and abiologic processes in banded iron formation genesis

Clark M. Johnson [a,*], Brian L. Beard [a], Cornelis Klein [b], Nic J. Beukes [c], Eric E. Roden [a]

[a] Department of Geology and Geophysics, University of Wisconsin, 1215 West Dayton Street, Madison, WI 53706, USA
[b] Department of Earth and Planetary Sciences, University of New Mexico, Albuquerque, NM 87131, USA
[c] Department of Geology, University of Johannesburg, Auckland Park 2006, Johannesburg, South Africa

Received 29 May 2007; accepted in revised form 18 October 2007; available online 26 October 2007

Abstract

The voluminous 2.5 Ga banded iron formations (BIFs) from the Hamersley Basin (Australia) and Transvaal Craton (South Africa) record an extensive period of Fe redox cycling. The major Fe-bearing minerals in the Hamersley–Transvaal BIFs, magnetite and siderite, did not form in Fe isotope equilibrium, but instead reflect distinct formation pathways. The near-zero average δ^{56}Fe values for magnetite record a strong inheritance from Fe^{3+} oxide/hydroxide precursors that formed in the upper water column through complete or near-complete oxidation. Transformation of the Fe^{3+} oxide/hydroxide precursors to magnetite occurred through several diagenetic processes that produced a range of δ^{56}Fe values: (1) addition of marine hydrothermal Fe^{2+}_{aq}, (2) complete reduction by bacterial dissimilatory iron reduction (DIR), and (3) interaction with excess Fe^{2+}_{aq} that had low δ^{56}Fe values and was produced by DIR. Most siderite has slightly negative δ^{56}Fe values of $\sim -0.5‰$ that indicate equilibrium with Late Archean seawater, although some very negative δ^{56}Fe values may record DIR. Support for an important role of DIR in siderite formation in BIFs comes from previously published C isotope data on siderite, which may be explained as a mixture of C from bacterial and seawater sources.

Several factors likely contributed to the important role that DIR played in BIF formation, including high rates of ferric oxide/hydroxide formation in the upper water column, delivery of organic carbon produced by photosynthesis, and low clastic input. We infer that DIR-driven Fe redox cycling was much more important at this time than in modern marine systems. The low pyrite contents of magnetite- and siderite-facies BIFs suggests that bacterial sulfate reduction was minor, at least in the environments of BIF formation, and the absence of sulfide was important in preserving magnetite and siderite in the BIFs, minerals that are poorly preserved in the modern marine record. The paucity of negative δ^{56}Fe values in older (Early Archean) and younger (Early Proterozoic) BIFs suggests that the extensive 2.5 Ga Hamersley–Transvaal BIFs may record a period of maximum expansion of DIR in Earth's history.

1. INTRODUCTION

Banded iron formations (BIFs) have played a prominent role in discussions on the surface environments of the ancient Earth because their origin requires redox conditions and iron transport pathways that were markedly different than those of the modern iron cycle (e.g., Trendall, 2002; Klein, 2005). The large inventory of Fe^{3+}-bearing oxides (magnetite, hematite) requires an oxidant during BIF genesis, given the fact that all proposed iron sources (riverine, marine hydrothermal) were Fe^{2+}. Contrary to common belief, however, hematite or goethite are not the major Fe-bearing phases in fresh BIFs that are absent the effects of weathering, supergene alteration, mineralization, or metamorphism (Simonson, 2003). Instead, Fe^{2+}-bearing minerals such as magnetite and siderite are the major

* Corresponding author. Fax: +1 608 262 0693.
E-mail address: clarkj@geology.wisc.edu (C.M. Johnson).

0016-7037/$ - see front matter © 2007 Elsevier Ltd. All rights reserved.
doi:10.1016/j.gca.2007.10.013

repositories of Fe in BIFs, reflecting the fact that the average oxidation state of iron in BIFs is $Fe^{2.4+}$ (e.g., Klein and Beukes, 1992). The sources and pathways for Fe^{2+}, therefore, are as important to models of BIF genesis as the oxidative pathways. The source of aqueous Fe^{2+} has been commonly argued to be marine hydrothermal systems, largely based on rare earth element (REE) data (e.g., Bau et al., 1997). REE data, however, do not directly constrain the Fe sources, nor the iron pathways involved in BIFs genesis.

The role of bacteria in BIF genesis has been extensively discussed because the period in which the major BIFs were deposited (~2.8 to 1.8 Ga) overlaps major changes that are thought to have occurred in the biosphere and atmosphere (Knoll, 2003; Canfield, 2005). Indirect roles for bacteria have been proposed, where Fe^{2+} oxidation occurred through elevated atmospheric O_2 produced by oxygenic photosynthesis (Cloud, 1968). A more direct role for bacteria might have involved Fe^{2+} oxidation that was metabolically coupled to reduction of CO_2 (Konhauser et al., 2002; Kappler et al., 2005):

$$4Fe^{2+} + 7H_2O + CO_2 \rightarrow CH_2O + 4FeOOH + 8H^+ \quad (1)$$

The ubiquitous magnetite and siderite in Late Archean to Early Proterozoic BIFs that have not been subjected to ore-forming processes or significant metamorphism are common end products of dissimilatory iron reduction (DIR) of ferric oxide/hydroxides by bacteria (Lovley et al., 1987), and a reductive role for bacteria in BIF genesis has been proposed (Nealson and Myers, 1990; Konhauser et al., 2005), which may be represented as the reverse of Eq. (1). Despite great speculation in the literature regarding the potential role of bacteria in BIF formation, clear evidence for bacterial processes in BIF genesis is essentially non-existent (Klein, 2005).

Here, we report new iron isotope data for the 2.50–2.45 Ga Brockman Iron Formation of the Hamersley Basin, Western Australia, one of the best preserved and most intensively studied BIFs in the world (Trendall and Blockley, 1970; Trendall et al., 2004). We compare these new data to our previous work on the Kuruman and Griquatown iron formations of the Transvaal Craton, South Africa (Johnson et al., 2003), which were deposited synchronously with the Brockman Iron Formation (Pickard, 2003). These results significantly expand the Fe isotope database on BIFs, which includes additional studies (Dauphas et al., 2004, 2007; Rouxel et al., 2005; Frost et al., 2006; Valaas-Hyslop et al., in press; Whitehouse and Fedo, 2007). Coupled with a growing database of experimentally determined Fe isotope fractionation factors, the results presented here provide new constraints on the Fe pathways that were involved in BIF formation, including evaluation of the role of bacteria in BIF genesis.

2. IRON PATHWAYS AND ISOTOPIC FRACTIONATIONS

Most models for BIF genesis involve Fe redox changes and mineral precipitation (e.g., Klein, 2005), and Fe isotope fractionation factors are now known for the key processes that were involved (Fig. 1). Iron isotope compositions are expressed in terms of $^{56}Fe/^{54}Fe$ ratios in units of per mil (‰), relative to the average of igneous rocks:

$$\delta^{56}Fe = (^{56}Fe/^{54}Fe_{Sample}/^{56}Fe/^{54}Fe_{Ig/Rxs} - 1)\ 10^3 \quad (2)$$

(Beard et al., 2003a). On this scale, the $\delta^{56}Fe$ value of the IRMM-014 standard is −0.09‰ (Beard et al., 2003a). Isotopic fractionations between two components, A and B, are described by:

$$\Delta^{56}Fe_{A-B} = \delta^{56}Fe_A - \delta^{56}Fe_B \sim 10^3 \ln \alpha_{A-B} \quad (3)$$

where α_{A-B} is the isotopic fractionation factor, following standard practice.

The very large quantities of Fe that are required for BIF deposition are generally thought to have been originally supplied by marine hydrothermal sources as Fe^{2+}_{aq} (pathway 1, Fig. 1). During oxidation of Fe^{2+}_{aq} to Fe^{3+}_{aq}, followed by precipitation of Fe^{3+}_{aq} to ferric oxide/hydroxide, the net isotopic fractionation between ferric oxide/hydroxide and initial Fe^{2+}_{aq} is ~+1.5‰ at room temperature (pathway 2, Fig. 1), reflecting a +2.9‰ Fe^{3+}_{aq}–Fe^{2+}_{aq} equilibrium fractionation and a ~−1.4‰ kinetic fractionation between ferric oxide/hydroxide and Fe^{3+}_{aq} upon precipitation; the later fractionation may vary on the order of ~1‰, depending upon precipitation kinetics (Beard and Johnson, 2004). The overall ferric oxide/hydroxide–Fe^{2+}_{aq} fractionation appears to be similar regardless of the oxidative pathway involved, including abiologic oxidation by O_2 (Bullen et al., 2001), anaerobic photosynthetic Fe^{2+} oxidation (Croal et al., 2004), oxidation by acidophilic iron-oxidizing bacteria (Balci et al., 2006), or UV-photo oxidation (Staton et al., 2006), where most of these fractionations measured in experiments vary between +1.0‰ and +2.0‰. Ferric oxide/hydroxides that are formed by only a few % oxidation and precipitation record the maximum fractionation, and hence will have $\delta^{56}Fe$ values that are ~1.5‰ higher than those of the initial Fe^{2+}_{aq}. In contrast, complete oxidation and precipitation will produce ferric oxide/hydroxides that have $\delta^{56}Fe$ values equal to those of the initial Fe^{2+}_{aq}, despite a significant $Fe(OH)_3$–Fe^{2+}_{aq} or Fe_2O_3–Fe^{2+}_{aq} fractionation factor. The $\delta^{56}Fe$ values of the flux of ferric oxide/hydroxides from the upper ocean layer to the seafloor (pathway 3, Fig. 1) will therefore be determined by the extent and rate of oxidation and precipitation that occurs in the upper part of the water column.

Transport of the ferric oxide/hydroxide "rain" into Fe^{2+}_{aq}-rich fluids in the deep marine anoxic layer produces opportunities for reactions that may produce important BIF minerals, including magnetite, via reactions such as:

$$2Fe(OH)_3 + Fe^{2+}_{aq} \rightarrow Fe_3O_4 + 2H_2O + 2H^+ \quad (4)$$

(pathway 4, Fig. 1). The Fe isotope composition of magnetite in the above reaction may, for example, reflect simple addition of Fe^{3+} and Fe^{2+} sources. Reaction of siderite and ferric hydroxides may also produce magnetite under burial metamorphic conditions, reflecting the same addition of Fe sources as given in Eq. (4). Dissimilatory Fe^{3+} reduction (DIR) may also produce Fe^{2+}_{aq} via the reverse of Eq. (1), or in the case of oxidation of acetate, reactions such as:

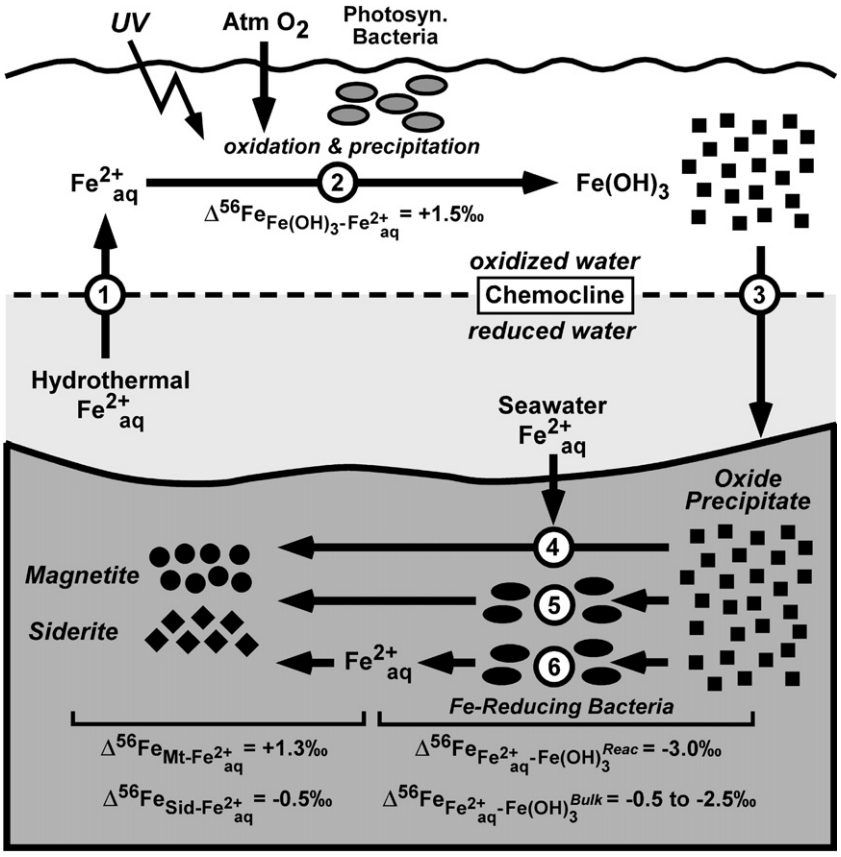

Fig. 1. Iron pathways and isotopic fractionations in banded iron formation (BIF) genesis. The primary iron source is inferred to be hydrothermal Fe^{2+}_{aq} (pathway 1), sourced to relatively anoxic deep water masses or shallow hydrothermal vents. Ascent of deep Fe^{2+}_{aq}-rich waters to the upper water column was accompanied by oxidation and formation of ferric oxide/hydroxide precipitates (pathway 2), which would have decreased Fe^{2+}_{aq} contents in the upper oceans, defining a chemocline that separated shallow oxidized waters from deep anoxic water; oxidation of upwelling Fe^{2+}_{aq} could have occurred by UV-photo oxidation, atmospheric O_2, or anaerobic photosynthetic Fe^{2+} oxidation. Partial oxidation will produce ferric oxide/hydroxide precipitates that have positive $\delta^{56}Fe$ values, controlled by the $Fe(OH)_3$–Fe^{2+}_{aq} fractionation factor and extent of reaction, whereas complete oxidation would produce no net isotopic change relative to the initial Fe^{2+}_{aq}. Settling of the ferric oxide/hydroxide "rain" from above the chemocline produced an Fe^{3+} flux (pathway 3) to the site of BIF deposition on the ocean floor. Conversion of precursor ferric oxide/hydroxides to magnetite at or below the sediment-water interface occurred via several pathways, including reactions with seawater Fe^{2+}_{aq} (pathway 4), reduction by dissimilatory Fe^{3+} reduction (DIR) under Fe^{2+}_{aq}-limited conditions (pathway 5), or DIR in the presence of excess Fe^{2+}_{aq} (pathway 6). In the case of pathway 6, the $\delta^{56}Fe$ values of the excess Fe^{2+}_{aq} will be controlled by the $Fe^{2+}_{aq} - Fe(OH)_3$ fractionation factor during DIR, where the $\delta^{56}Fe$ value for Fe^{2+}_{aq} is controlled by the proportions of reactive and bulk $Fe(OH)_3$, as well as the Fe^{2+} inventory (Crosby et al., 2007). The $\delta^{56}Fe$ values of magnetite and siderite that formed in the presence of excess Fe^{2+}_{aq} will be controlled by the magnetite–Fe^{2+}_{aq} and siderite–Fe^{2+}_{aq} fractionation factors, respectively.

$$CH_3COO^- + 8Fe(OH)_3 \rightarrow 8Fe^{2+}_{aq} + 2HCO_3^- + 15OH^- + 5H_2O \quad (5)$$

Fe^{2+}_{aq} produced by reaction 5 could be transported over space and time to produce magnetite via reaction 4. Complete conversion of ferric oxide/hydroxide to magnetite may consume all Fe^{2+} produced by DIR, which may in turn produce no net change in $\delta^{56}Fe$ values between initial ferric oxide/hydroxide and the magnetite product (pathway 5, Fig. 1). "Excess" Fe^{2+} is common, however, during DIR prior to magnetite formation (e.g., Johnson et al., 2005), and Fe^{2+}_{aq} produced by DIR may exist in pore fluids in modern marine sediments (e.g., Severmann et al., 2006). The $\delta^{56}Fe$ values of Fe^{2+}_{aq} produced by DIR are always lower than those of the initial ferric oxide/hydroxide (pathway 6, Fig. 1), reflecting a −3.0‰ equilibrium fractionation between Fe^{2+}_{aq} and a reactive Fe^{3+} layer on the ferric oxide/hydroxide surface (Crosby et al., 2005, 2007). The absolute $\delta^{56}Fe$ values for Fe^{2+}_{aq} produced by DIR may range from −0.5‰ to −2.5‰ relative to the initial ferric oxide/hydroxide (Beard et al., 1999, 2003a; Icopini et al., 2004; Crosby et al., 2005, 2007; Johnson et al., 2005), and are primarily controlled by the relative proportions of $Fe^{2+}_{aq}$and the reactive Fe^{3+} surface layer during reduction (Crosby et al., 2007).

In the presence of excess Fe^{2+}_{aq}, the $\delta^{56}Fe$ values of magnetite and siderite may be controlled by the fluid-mineral isotope fractionation factors, rather than simple addition reactions such as Eq. (4). Under equilibrium conditions, the magnetite–Fe^{2+}_{aq} fractionation factor is estimated to be +1.3‰ at room temperature (Johnson et al., 2005) (Fig. 1). In contrast, the equilibrium siderite–

Fe^{2+}_{aq} fractionation factor at room temperature is estimated to be −0.5‰ (Wiesli et al., 2004) (Fig. 1). The ankerite–Fe^{2+}_{aq} fractionation factor is estimated to be more negative, based on natural samples (Johnson et al., 2003), experiments that involved 15 mol % Ca substitution into siderite (Johnson et al., 2005), and predicted fractionation factors as calculated from theory (Polyakov and Mineev, 2000).

3. SAMPLING AND ANALYTICAL METHODS

Samples of the Brockman Iron Formation, Hamersley Basin, Australia, were obtained from a core from hole DDH-44 near Paraburdo (Ewers and Morris, 1981). Previous stable isotope studies of this core suggest burial metamorphism between 60 and 160 °C, significantly lower than in other parts of the Hamersley Basin (Kaufman et al., 1990). Definitions of macrobands rich in oxides and Fe carbonate (BIF macrobands) and those that are shale rich (S macrobands) are based on correlation to the type section (Trendall and Blockley, 1970). Milligram-size samples were taken from fresh core surfaces that had been cleaned in distilled water, using a tungsten–carbide bit. Based on image analysis using matching thin sections, only siderite and magnetite layers that were >95% monomineralic were sampled. The powdered samples were decomposed by mixed acid digestion ($HF–HNO_3$) and purified for Fe using anion-exchange chromatography (Beard et al., 2003a). Isotopic compositions of Fe were measured using MC-ICP-MS (multi-collector, inductively-coupled plasma mass spectrometry; Micromass *IsoProbe*) at the University of Wisconsin, Madison. Twenty-six samples used in this study were analyzed at least two times, and these repeat measurements differ by an average of 0.05‰, which is essentially identical to the reproducibility obtained on pure standards. Seven mesobands (~cm thick) were sampled at the mm-scale in duplicate or triplicate to assess fine-scale sample heterogeneity. Additional details on chemical separations and mass analysis methods may be found in Beard et al. (2003a) and Albarede and Beard (2004).

4. RESULTS

New iron isotope data (Table 1 and Fig. 2) for the 2.50–2.45 Ga Brockman Iron Formation of the Hamersley Basin, Western Australia (Trendall and Blockley, 1970) span a range in $\delta^{56}Fe$ values that is similar to that defined by the synchronously deposited Kuruman and Griquatown iron formations of the Transvaal Craton, South Africa (Johnson et al., 2003), as well as several BIF samples of 1.9 and 2.7 Ga age from other localities (Rouxel et al., 2005; Frost et al., 2006; Valaas-Hyslop et al., in press). The $\delta^{56}Fe$ values of magnetite and siderite broadly overlap in the Australian and South African suites, although the average Fe isotope compositions for these minerals are distinct. The average $\delta^{56}Fe$ value for magnetite is −0.02‰, which is indistinguishable from average continental crust (Beard et al., 2003a,b; Beard and Johnson, 2006), whereas the average $\delta^{56}Fe$ value for siderite is −0.60‰, significantly

Table 1
Fe isotope data for the Brockman Iron Formation

Sample	Mineral	$\delta^{56}Fe$	$\delta^{57}Fe$
Brockman Iron Formation			
Dales Gorge Member			
Sample 2-2, BIF-5, 42.7 m			
2-2-1	Mt	−0.31 ± 0.04	−0.42 ± 0.06
repeat		−0.24 ± 0.04	−0.32 ± 0.02
2-2-2	Sid	−0.14 ± 0.04	−0.23 ± 0.03
repeat		−0.20 ± 0.05	−0.29 ± 0.03
2-2-3	Sid	−0.66 ± 0.04	−0.94 ± 0.03
repeat		−0.59 ± 0.04	−0.84 ± 0.02
2-2-4	Sid	−0.68 ± 0.04	−1.00 ± 0.04
2-2-5	Mt	0.16 ± 0.04	0.21 ± 0.03
repeat		0.26 ± 0.03	0.40 ± 0.03
2-2-6	Mt	−0.37 ± 0.03	−0.55 ± 0.03
2-2-7	Sid	−1.08 ± 0.04	−1.63 ± 0.03
repeat		−1.13 ± 0.03	−1.60 ± 0.03
repeat		−1.10 ± 0.06	−1.59 ± 0.03
2-2-8	Sid	−1.17 ± 0.05	−1.69 ± 0.03
2-2-9	Mt	−0.51 ± 0.04	−0.80 ± 0.03
2-2-10	Mt	−0.07 ± 0.04	−0.07 ± 0.03
2-2-12	Mt	−0.61 ± 0.03	−0.93 ± 0.03
2-2-13	Mt	0.19 ± 0.04	0.33 ± 0.03
repeat		0.11 ± 0.03	0.15 ± 0.03
2-2-14	Mt	−0.22 ± 0.06	−0.33 ± 0.04
repeat		−0.17 ± 0.04	−0.28 ± 0.02
2-2-15	Sid	−1.05 ± 0.03	−1.53 ± 0.03
2-2-16	Sid	−1.05 ± 0.04	−1.55 ± 0.03
2-2-17	Sid	−1.07 ± 0.03	−1.47 ± 0.03
2-2-19	Mt	−0.27 ± 0.04	−0.41 ± 0.04
Sample 3-3, BIF-5, 43.9 m			
3-3-1-A	Mt	−1.16 ± 0.04	−1.70 ± 0.03
repeat		−1.21 ± 0.04	−1.75 ± 0.03
3-3-1-B	Mt	−0.29 ± 0.04	−0.42 ± 0.04
repeat		−0.33 ± 0.05	−0.41 ± 0.04
3-3-1-C	Mt	−0.26 ± 0.04	−0.46 ± 0.03
repeat		−0.29 ± 0.09	−0.42 ± 0.02
3-3-2	Sid	−0.28 ± 0.05	−0.39 ± 0.03
3-3-3	Mt	−0.40 ± 0.03	−0.55 ± 0.03
3-3-4	Mt	−0.26 ± 0.03	−0.34 ± 0.03
3-3-5	Mt	−0.50 ± 0.06	−0.77 ± 0.04
3-3-6	Sid	−1.22 ± 0.04	−1.80 ± 0.04
3-3-7	Sid	−1.36 ± 0.05	−2.03 ± 0.04
3-3-8	Mt	−0.37 ± 0.04	−0.52 ± 0.03
repeat		−0.32 ± 0.04	−0.52 ± 0.04
3-3-9	Mt	−0.53 ± 0.03	−0.83 ± 0.03
3-3-10	Sid	−1.36 ± 0.09	−1.96 ± 0.04
3-3-11	Sid	−1.30 ± 0.04	−1.93 ± 0.03
3-3-12	Mt	−0.71 ± 0.03	−1.07 ± 0.02
3-3-13-A	Sid	−2.06 ± 0.07	−2.83 ± 0.03
repeat		−2.06 ± 0.03	−2.94 ± 0.03
3-3-13-B	Sid	−1.50 ± 0.05	−2.07 ± 0.03
repeat		−1.56 ± 0.04	−2.24 ± 0.04
3-3-13-C	Sid	−1.57 ± 0.03	−2.34 ± 0.03
3-3-14	Mt	−0.44 ± 0.03	−0.69 ± 0.03
3-3-15	Sid	−1.18 ± 0.03	−1.75 ± 0.04
3-3-16	Sid	−1.07 ± 0.03	−1.58 ± 0.02
3-3-17-A	Mt	−0.03 ± 0.03	0.03 ± 0.03
3-3-17-B	Mt	0.03 ± 0.05	0.05 ± 0.03
3-3-18	Sid	−0.62 ± 0.03	−0.88 ± 0.03
3-3-19	Mt	−0.22 ± 0.05	−0.34 ± 0.04
3-3-20	Sid	−1.05 ± 0.04	−1.49 ± 0.03

Table 1 (*continued*)

Sample	Mineral	δ^{56}Fe	δ^{57}Fe
Sample 4-8, BIF-5, 44.2 m			
4-8-1	Sid	−0.89 ± 0.03	−1.28 ± 0.03
repeat		−0.86 ± 0.05	−1.22 ± 0.03
4-8-2	Mt	0.21 ± 0.04	0.27 ± 0.04
repeat		0.17 ± 0.03	0.27 ± 0.03
4-8-3	Mt	0.10 ± 0.02	0.10 ± 0.02
4-8-4	Sid	−1.12 ± 0.04	−1.67 ± 0.03
repeat		−1.12 ± 0.04	−1.61 ± 0.02
4-8-5	Mt	0.00 ± 0.04	−0.05 ± 0.03
repeat		0.01 ± 0.04	0.16 ± 0.05
4-8-6	Sid	−0.93 ± 0.03	−1.34 ± 0.02
repeat		−0.96 ± 0.04	−1.40 ± 0.03
4-8-7	Sid	−1.07 ± 0.10	−1.56 ± 0.04
4-8-8	Sid	−0.87 ± 0.03	−1.26 ± 0.03
4-8-9	Mt	0.27 ± 0.03	0.33 ± 0.02
4-8-10	Sid	−0.51 ± 0.03	−0.76 ± 0.03
4-8-11	Sid	−0.91 ± 0.03	−1.38 ± 0.03
Sample 6-2, S-6, 47.2 m			
6-2-1	Mt	0.84 ± 0.04	1.25 ± 0.03
repeat		0.79 ± 0.05	1.16 ± 0.04
repeat		0.80 ± 0.05	1.18 ± 0.04
repeat		0.77 ± 0.06	1.10 ± 0.03
6-2-2	Sid (impure)	0.02 ± 0.03	0.01 ± 0.03
6-2-3	Mt	0.67 ± 0.04	0.98 ± 0.03
repeat		0.61 ± 0.03	0.90 ± 0.03
6-2-4	Sid	0.35 ± 0.03	0.52 ± 0.03
6-2-5	Sid	0.15 ± 0.03	0.34 ± 0.02
6-2-6	Mt	0.73 ± 0.03	1.09 ± 0.03
6-2-7	Sid	−0.05 ± 0.02	−0.02 ± 0.02
Sample 16-7, BIF-13, 100.6 m			
16-7-1	Mt	0.32 ± 0.03	0.48 ± 0.02
repeat		0.34 ± 0.03	0.52 ± 0.03
16-7-2	Hem+chert	0.19 ± 0.07	0.26 ± 0.06
16-7-3	Sid	−0.12 ± 0.03	−0.16 ± 0.03
16-7-4	Mt	0.30 ± 0.03	0.47 ± 0.03
16-7-5	Mt	0.41 ± 0.03	0.59 ± 0.03
16-7-6	Sid	0.39 ± 0.05	0.60 ± 0.03
repeat		0.42 ± 0.03	0.55 ± 0.03
Sample 18-2, BIF-13, 103.6 m			
18-2-1	Sid	−0.80 ± 0.05	−1.17 ± 0.05
repeat		−0.91 ± 0.04	−1.35 ± 0.05
18-2-2	Mt (impure)	−0.12 ± 0.03	−0.15 ± 0.03
18-2-4	Sid	−0.76 ± 0.02	−1.19 ± 0.03
18-2-6	Sid	−0.81 ± 0.03	−1.21 ± 0.02
repeat		−0.74 ± 0.06	−1.15 ± 0.05
18-2-7	Mt	−0.02 ± 0.05	0.02 ± 0.03
18-2-8	Mt	0.02 ± 0.03	0.03 ± 0.03
repeat		−0.04 ± 0.03	−0.10 ± 0.02
18-2-9	Sid	−0.69 ± 0.05	−1.03 ± 0.06
18-2-10	Sid	−0.48 ± 0.06	−0.71 ± 0.03
18-2-11	Mt	0.07 ± 0.02	0.11 ± 0.02
18-2-13	Mt	0.10 ± 0.03	0.14 ± 0.03
18-2-14	Sid	−0.59 ± 0.03	−0.84 ± 0.02
18-2-15	Sid	−0.66 ± 0.06	−0.97 ± 0.03
18-2-17	Sid	−0.76 ± 0.08	−1.05 ± 0.05
18-2-18	Sid	−0.66 ± 0.04	−1.00 ± 0.04
Sample 20-4, BIF-14, 109.7 m			
20-4-1	Mt	1.19 ± 0.09	1.63 ± 0.04
20-4-2-A	Sid	0.04 ± 0.08	0.15 ± 0.05
20-4-2-B	Sid	0.63 ± 0.03	0.94 ± 0.03
20-4-4	Sid	1.00 ± 0.03	1.53 ± 0.03
20-4-5	Mt	1.12 ± 0.04	1.69 ± 0.03
Sample 30-9, BIF-16, 131.1 m			
30-9-1	Mt	−1.06 ± 0.03	−1.59 ± 0.03
30-9-2	Mt+Fe sil	−0.42 ± 0.03	−0.66 ± 0.03
30-9-3	Mt+Fe sil	−0.56 ± 0.02	−0.78 ± 0.02
30-9-4	Mt	−0.17 ± 0.02	−0.21 ± 0.02
30-9-5	Mt	0.02 ± 0.03	0.02 ± 0.02
30-9-7	Sid	−0.90 ± 0.03	−1.31 ± 0.02
30-9-8	Mt	−0.03 ± 0.09	−0.01 ± 0.05
30-9-9	Sid	−0.23 ± 0.03	−0.40 ± 0.03
30-9-10	Sid	−1.19 ± 0.03	−1.84 ± 0.03
Sample 35-9, BIF-16, 134.1 m			
35-4-1	Mt	0.05 ± 0.02	0.03 ± 0.03
35-4-2	Sid	−0.04 ± 0.03	−0.11 ± 0.02
Sample 37-11, BIF-16, 135.6 m			
37-11-1-A	Sid + chert	−0.93 ± 0.03	−1.32 ± 0.03
repeat		−0.84 ± 0.04	−1.21 ± 0.02
37-11-1-B	Sid + chert	−1.10 ± 0.04	−1.56 ± 0.02
repeat		−1.19 ± 0.04	−1.71 ± 0.03
37-11-2	Mt	−0.01 ± 0.03	0.02 ± 0.02
repeat		−0.09 ± 0.03	−0.17 ± 0.04
Joffre Member			
Sample 38-1, 182.9 m			
38-1-2	Sid	−1.12 ± 0.04	−1.63 ± 0.05
38-1-4	Sid	−0.29 ± 0.03	−0.33 ± 0.03
38-1-6	Sid	−0.10 ± 0.04	−0.14 ± 0.04
Sample 40-10, 185.9 m			
40-10-1-A	Sid	−0.85 ± 0.05	−1.28 ± 0.05
40-10-1-B	Sid	−0.22 ± 0.03	−0.34 ± 0.03
40-10-1-C	Sid	−0.59 ± 0.08	−0.85 ± 0.02
40-10-4-A	Sid	−0.67 ± 0.03	−0.95 ± 0.02
40-10-4-B	Sid	−0.18 ± 0.05	−0.19 ± 0.03

Note: δ^{56}Fe and δ^{57}Fe values reported as ^{56}Fe/^{54}Fe and ^{57}Fe/^{54}Fe ratios, respectively, relative to the average of igneous rocks (Beard et al., 2003a). On this scale, the δ^{56}Fe value of the IRMM-14 standard is −0.09. Core sample from hole DDH-44 (Ewers and Morris, 1981). BIF- and S-macrobands and stratigraphic height above the base of the Brockman Iron Formation based on correlation to the type section of Trendall and Blockley (1970). Each sample is from a distinct mesoband. "repeat" notes duplicate mass analysis of same solution on different day. "A", "B", "C", etc., notes duplicate sampling of same mesoband in sample. "Mt", magnetite; "Sid", siderite; "Fe Sil", Fe silicates; mineral bands >95% monomineralic unless noted.

lower than the average of igneous rocks or average continental crust. A χ^2 test of the magnetite and siderite Fe isotope data indicates that there is less than a 0.5% and 0.001% probability, respectively, that the distribution of these δ^{56}Fe values is Gaussian.

A first-order observation is that there are very large ranges in δ^{56}Fe values for both magnetite and siderite over restricted stratigraphic intervals (Fig. 2). Individual core samples (~10 cm in length) may have significant mm- to cm-scale variations in δ^{56}Fe values, but some core samples

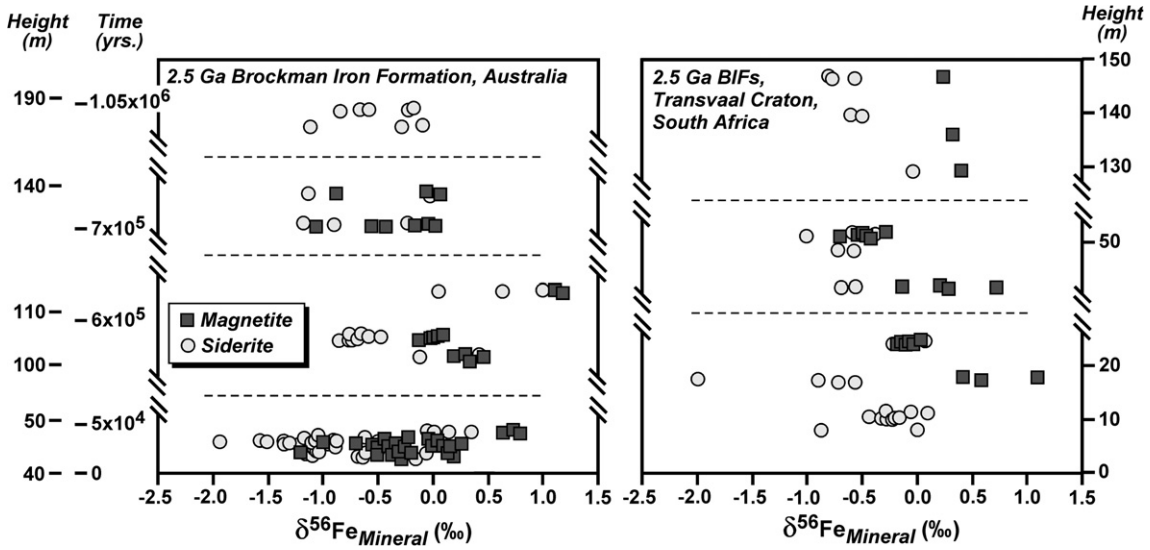

Fig. 2. Iron isotope data for siderite and magnetite from the Brockman Iron Formation (this study; Table 1) and the temporally correlative Kuruman and Griquatown iron formations from the Transvaal Craton, South Africa (Johnson et al., 2003). Stratigraphic heights relative to the base of the Brockman and Kuruman iron formations are shown. Dashed horizontal lines indicate scale breaks in stratigraphic height. Timescale for deposition of the Brockman Iron Formation shown at left, based on the BIF depositional rate of 180 m/m.y. (compacted sediment) from Trendall et al. (2004).

are more homogeneous at this scale; representative examples are shown in Fig. 3. Where individual cores have relatively large variability, the average δ^{56}Fe values for magnetite and siderite tend to be the lowest (e.g., cores 2-2 and 3-3, Fig. 3), whereas cores that have a more restricted range in Fe isotope compositions tend to have higher δ^{56}Fe values for magnetite and siderite (e.g., core 18-2, Fig. 3). Combing the data from Johnson et al. (2003), there is a weak negative correlation between the standard deviation of δ^{56}Fe values for magnetite from a specific core sample and the average δ^{56}Fe value for each core ($R^2 = 0.2$). The range in δ^{56}Fe values measured for magnetite in individual cores is less than that determined by Whitehouse and Fedo (2007), who report significant Fe isotope variations of up to 2‰ on the mm scale in 3.8 Ga BIFs from Isua, Greenland.

5. DISCUSSION

We divide our discussion into four parts. Our first focus is on the likely Fe isotope compositions of marine hydrothermal Fe^{2+}_{aq} in the Archean, inasmuch as these compositions define the δ^{56}Fe values of the primary source of Fe in BIFs. Second, we address the constraints that fine-scale isotopic heterogeneity place on the degree to which the Fe isotope compositions reflect equilibrium with seawater. Third, oxidation and precipitation processes in the upper water column are discussed in terms of the likely δ^{56}Fe values of the $Fe(OH)_3$ flux from the upper water column to the ocean floor. Fourth, the Fe pathways and isotopic fractionations involved in early diagenetic processes at or near the sediment-water interface during BIF formation are discussed, with a focus on magnetite and siderite formation. We conclude with a discussion of the factors that may have led to large-scale magnetite and siderite formation in Archean and Early Proterozoic BIFs.

5.1. The isotopic composition of marine hydrothermal Fe^{2+}_{aq}

Constraining the Fe isotope composition of the marine hydrothermal Fe^{2+}_{aq} flux (pathway 1, Fig. 1) is an important first step in defining the expected range in δ^{56}Fe values for the initial ferric oxide/hydroxide precipitates that formed in the upper water column that are ultimately transported to the ocean floor. Although modern marine hydrothermal fluids have δ^{56}Fe values between −0.8‰ and −0.1‰, the positive correlation between δ^{56}Fe and Fe content (Fig. 4A) indicates that the mass-weighted δ^{56}Fe value of the modern marine hydrothermal flux lies closer to the high end of this range at $\delta^{56}Fe = -0.23$‰, based on the data available. The higher Fe-content samples in modern marine hydrothermal fluids presumably reflect higher extents of oceanic crust dissolution and/or minimal fluid evolution prior to exhalation. The lower δ^{56}Fe values for low-Fe fluids in the modern oceans likely reflect near-vent oxidation and precipitation upon exhalation (Severmann et al., 2004; Chu et al., 2006), but in an anoxic, Fe^{2+}_{aq}-rich Archean ocean, oxidation close to the vent should have been minimal.

If marine hydrothermal fluxes were higher in the Archean (e.g., Bau and Möller, 1993), reflecting higher heat flow, we would expect greater extents of oceanic crust dissolution than today, shifting the mass-weighted δ^{56}Fe values closer toward the isotopic composition of bulk oceanic crust. Because fluid-mineral Fe isotope fractionation factors decrease with increasing temperature for oceanic crust alteration reactions (Fig. 4B), a higher heat-flow regime in the Archean would also shift the δ^{56}Fe values for marine

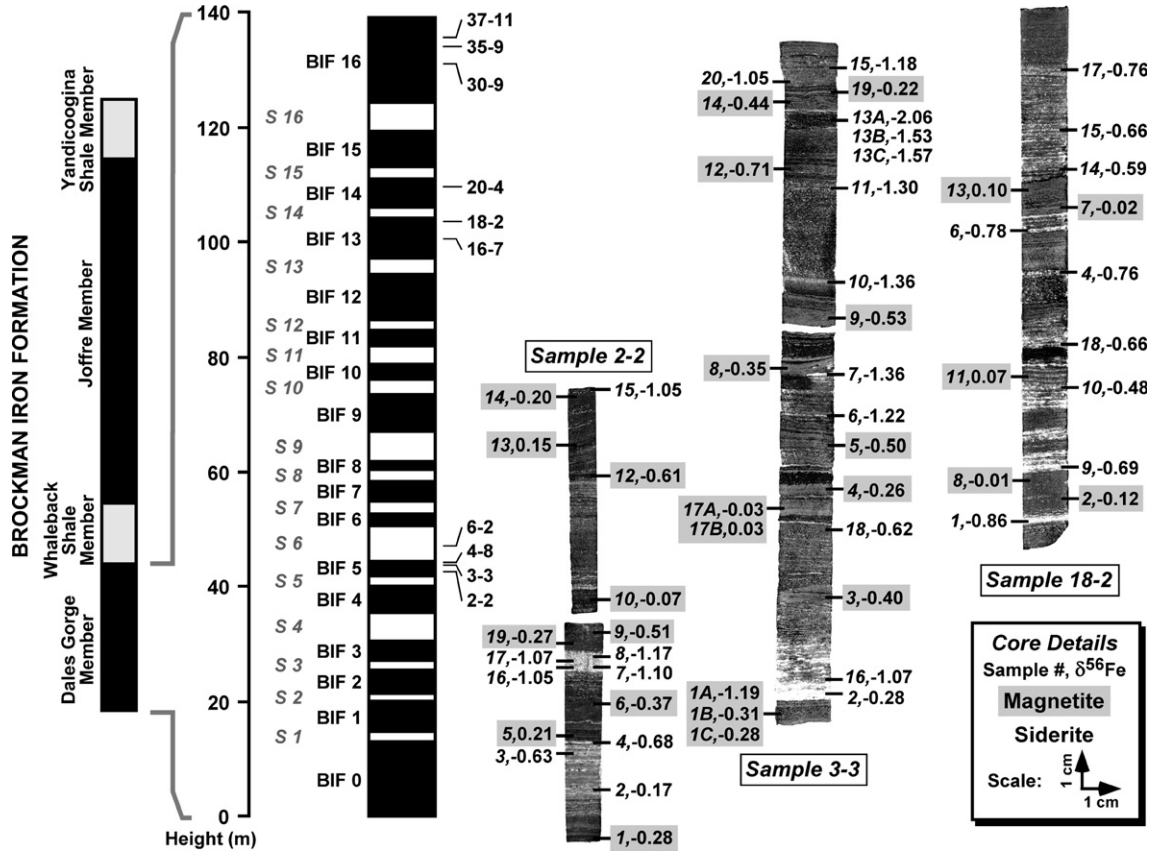

Fig. 3. Stratigraphic section of the Brockman Iron Formation illustrating BIF samples analyzed in this study, including selected annotated core images. Stratigraphic section based on scaling the DDH-44 section that was analyzed to the type section of the Brockman Iron Formation (Trendall and Blockley, 1970). Stratigraphic position of samples analyzed in this study (2-2, 3-3, 4-8, 6-2, 16-7, 18-2, 20-4, 30-9, 35-9, and 37-11) is noted. Representative core images shown on right side of diagram for samples 2-2, 3-3, and 18-2. Samples 2-2 and 3-3 illustrate fine-scale Fe isotope heterogeneity, which is most common for samples that have δ^{56}Fe values for magnetite less than zero. Sample 18-2 illustrates a core sample that has relatively homogeneous Fe isotope compositions, which are generally associated with samples that have δ^{56}Fe values for magnetite that are near zero. The average $\delta^{56}Fe_{Magnetite}$ value for cores 2-2, 3-3, and 18-2 are -0.22 ± 0.28‰, -0.38 ± 0.37, and 0.00 ± 0.09, respectively (all errors 1 SD). The average $\delta^{56}Fe_{Siderite}$ values for cores 2-2, 3-3, and 18-2 are -0.87 ± 0.34, -1.15 ± 0.43, and -0.69 ± 0.11, respectively. All core images scaled to the same vertical and horizontal scale (1 cm scale noted in gray box). Sample numbers and δ^{56}Fe values noted for magnetite (in gray boxes) and siderite.

hydrothermal Fe^{2+}_{aq} toward zero. For simplicity, therefore, we assume that the mass-weighted marine hydrothermal Fe^{2+}_{aq} flux during BIF genesis had a δ^{56}Fe value of zero; changing this by a few tenths per mil will not significantly affect our conclusions.

5.2. Fine-scale isotopic heterogeneity: diagenesis or changes in seawater?

Large changes in δ^{56}Fe values over short time intervals are recorded in Late Archean and Early Proterozoic sedimentary rocks, which lead Rouxel et al. (2005) and Anbar and Rouxel (2007) to propose that the Fe isotope compositions of seawater varied greatly in response to oxide precipitation in BIFs, or possibly oxides dispersed on continental shelves. Our results provide a test of this proposal because the depositional rates of the Hamersley Basin BIFs are known from geochronology (Trendall et al., 2004), providing constraints on the timescales over which Fe isotope compositions may have varied in Late Archean and Early Proterozoic marine sedimentary environments. The temporal variation in δ^{56}Fe values measured for three closely-spaced core samples of the Dales Gorge member of the Brockman Iron Formation that represent ~15 kyr of deposition are compared in Fig. 5 with data from late Quaternary marine sediments from the Rainbow vent site, Mid-Atlantic Ridge (Severmann et al., 2004) that were deposited over a similar time interval. Over the timescale that this comparison represents, the hydrogenous Fe components of the Rainbow sediments remain constant in their δ^{56}Fe values (Fig. 5). In addition, the maximum rate of change measured for Cenozoic Fe–Mn crusts (0.25‰/100 kyr; Chu et al., 2006) is shown in Fig. 5, and over the 15 kyr depositional interval of the Rainbow sediments and the BIF samples, the maximum observed rate of change for Fe–Mn crusts produces negligible changes in δ^{56}Fe values. The relative constancy in δ^{56}Fe values for recent marine systems over ~15 kyr stands in marked contrast to the

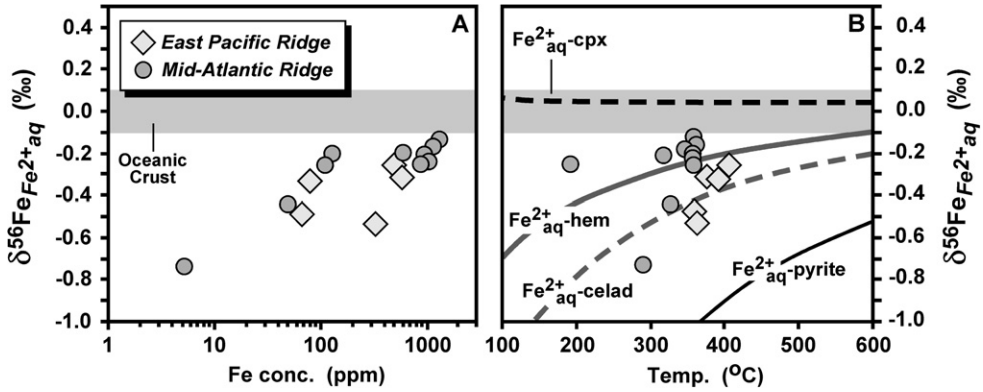

Fig. 4. Variations in δ^{56}Fe values and Fe contents (A) and exhalation temperatures (B) for modern marine hydrothermal vent fluids. Bulk oceanic crust has δ^{56}Fe values that lie between −0.1 and +0.1‰ (Beard et al., 2003a; Rouxel et al., 2003; Poitrasson et al., 2004), and vent fluids that have the highest Fe contents approach the Fe isotope composition of bulk oceanic crust. Most vent fluids that have been analyzed for Fe isotope compositions have exhalation temperatures between 300 and 400 °C, and fluid-mineral fractionation factors in this temperature range indicate that Fe^{2+}_{aq} in equilibrium with various secondary minerals (hematite, celadonite, and pyrite) should have modestly negative δ^{56}Fe values, assuming these minerals have δ^{56}Fe of zero. Data from Beard et al. (2003b) and Severmann et al. (2004). Fluid-mineral fractionation factors from Polyakov and Mineev (2000) and Schauble et al. (2001).

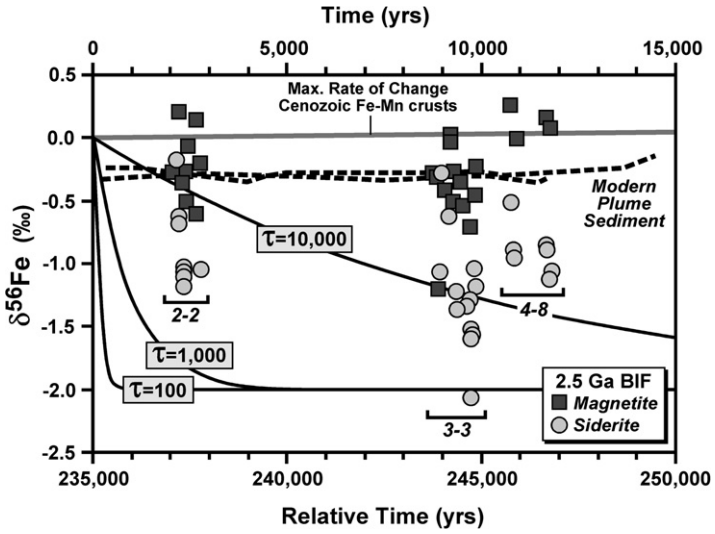

Fig. 5. Comparison of temporal Fe isotope variations in modern marine environments and three core samples from the Dales Gorge member of the Brockman Iron Formation that reflect deposition over a 15 kyr period. Black dashed line represents data for modern hydrogenous sediment from the Mid-Ocean Ridge hydrothermal plume at the Rainbow vent site shown for two cores (Severmann et al., 2004), where ages are based on radiocarbon geochronology (top scale). Near-horizontal gray line represents the maximum rate of change in Fe isotope compositions measured for Cenozoic Fe–Mn crusts, as plotted over the 15 kyr. interval, from the data of Chu et al. (2006) (age constraints provided by ^{10}Be; top scale). In contrast to the essentially invariant Fe isotope compositions over 15 kyr. from modern marine settings, Fe isotope compositions of the Dales Gorge samples vary greatly for both magnetite and siderite. Relative time in years for the BIF samples (lower scale) calculated relative to the base of the section using the deposition rates determined by Trendall et al. (2004). Also shown are Fe isotope curves calculated for various Fe residence times, as described in Johnson et al. (2003), reflecting the response to an instantaneous 2‰ decrease in the input δ^{56}Fe values to seawater. Collectively, these relations, as well as the comparison of data from modern marine environments to those of the 2.5 Ga BIFs, suggests that the wide range in δ^{56}Fe values in the BIFs cannot reflect changes in the Fe isotope compositions of Late Archean or Early Proterozoic seawater.

large variations in δ^{56}Fe values that are recorded by magnetite and siderite from the Dales Gorge BIF over a comparable time span (Fig. 5).

The wide range in δ^{56}Fe values for the Dales Gorge BIFs over short time intervals is opposite that predicted by the longer Fe residence times expected for the Late Archean and Early Proterozoic oceans if the BIFs directly reflect the Fe isotope compositions of seawater. Rapid changes in seawater δ^{56}Fe values can only occur if the Fe residence times are short (<100 years), such as those estimated for the modern oceans based on Fe concentrations (~0.01 ppm; e.g., Rue and Bruland, 1995) and fluxes ($\sim 5 \times 10^{12}$ mol/yr; e.g., Canfield and Raiswell, 1999). Even in the modern oceans, however, the relations in Fig. 5 suggest that mini-

mal changes in δ^{56}Fe values for seawater occur over ~15 kyr timescales, so it seems unlikely that the range in δ^{56}Fe values for the Dales Gorge BIF samples that have significant isotopic heterogeneity directly reflect those of seawater. Archean seawater is estimated to have contained between 2 and 50 ppm Fe (Ewers, 1983; Sumner, 1997; Canfield, 2005), which would produce an Fe residence time between 10,600 and 236,000 years, using the fluxes of Canfield and Raiswell (1999). Similarly rapid changes in δ^{56}Fe values may be inferred from data obtained on sedimentary pyrite from the 2.7 Ga Belingwe sedimentary basin (Zimbabwe), where Archer and Vance (2006) noted that δ^{56}Fe values vary by 2‰ over a 10 cm interval. It therefore seems likely that the large range in δ^{56}Fe values in Late Archean and Early Proterozoic BIFs and other sedimentary rocks and sulfides reflects a strong early diagenetic component, particularly for samples that have fine-scale isotopic variability.

The Fe isotope compositions of magnetite and siderite from adjacent bands (generally <1 cm apart) indicate that these minerals did not generally form in Fe isotope equilibrium (Fig. 6). Magnetite and siderite that formed in Fe isotope equilibrium at room temperature should lie along a magnetite–siderite fractionation line of +1.8‰ (Wiesli et al., 2004; Johnson et al., 2005), but this is not the case for any of the adjacent magnetite–siderite bands in the BIFs from the Hamersley Basin or Transvaal Craton (Fig. 6). In addition, the δ^{56}Fe values calculated for Fe^{2+}_{aq} based on fluid-mineral fractionation factors are significantly different than those estimated for Archean seawater (Fig. 6). A number of siderites have calculated δ^{56}Fe values for Fe^{2+}_{aq} that lie near-zero, which overlaps the estimates for Archean seawater, but the δ^{56}Fe values calculated for Fe^{2+}_{aq} based on magnetite are significantly lower in almost all cases.

The lack of apparent low-temperature Fe isotope equilibrium is probably not due to metamorphism or burial diagenesis. Although isotopic equilibration at higher temperatures would decrease the magnetite–siderite Fe isotope fractionation, temperatures in excess of 400 °C would be required to produce the average magnetite–siderite fractionation of +0.5‰ to +0.6‰ (Polyakov and Mineev, 2000; Polyakov et al., 2007), which is inconsistent with the low grades of metamorphism of the Hamersley Basin samples (Kaufman et al., 1990), as well as the Transvaal Craton samples (Miyano and Beukes, 1984). It is important to note that many of the Fe carbonates analyzed are ankeritic, based on electron microprobe and bulk chemical analyses of other samples from the same core (Klein and Beukes, 1989; Kaufman et al., 1990); to the degree that the magnetite–carbonate pairs in Fig. 6 include ankerite, isotopic disequilibrium is even more pronounced because Ca substitution increases the magnetite–Fe carbonate fractionation factor (Polyakov and Mineev, 2000; Johnson et al., 2005).

The offset in the array of δ^{56}Fe values for magnetite and siderite relative to that expected for isotopic equilibrium is interpreted to reflect the combined effects of partial isotopic equilibrium and the isotopic composition of the Fe that was transported to individual layers. If, for example, the δ^{56}Fe values of siderite and magnetite from adjacent bands were entirely controlled by the isotopic compositions of the Fe that was transported to these layers, the data should fall along a 1:1 line in Fig. 6, assuming that the δ^{56}Fe values

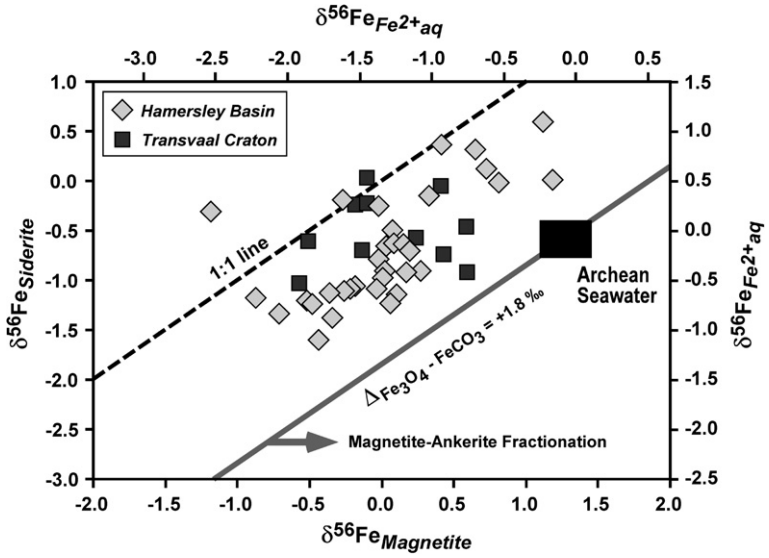

Fig. 6. Comparison of Fe isotope compositions of magnetite and siderite from adjacent bands (generally <1 cm apart) in BIFs from the Hamersley Basin (this study) and Transvaal Craton (Johnson et al., 2003). Also shown are calculated δ^{56}Fe values for Fe^{2+}_{aq} that would be in equilibrium with magnetite and siderite, using the magnetite–Fe^{2+}_{aq} fractionation factor from Johnson et al. (2005) and the siderite–Fe^{2+}_{aq} fractionation factor from Wiesli et al. (2004); combined, these predict a magnetite–siderite fractionation factor of +1.8‰, but none of the magnetite-siderite pairs plot along this line, indicating that they did not form in isotopic equilibrium, nor from a common fluid. The magnetite–ankerite fractionation line will lie to the right of the magnetite–siderite fractionation line (Polyakov and Mineev, 2000; Johnson et al., 2005).

for the delivered Fe was the same for adjacent bands. That the data scatter between a 1:1 line and the line that reflects isotopic equilibrium indicates that any model proposed to explain the Fe isotope compositions of the 2.5 Ga BIFs from the Hamersley Basin and Transvaal Craton must include pathway-dependent processes, as well as equilibrium processes.

5.3. Oxidation and precipitation in the upper water column

It is generally accepted that the 2.5 Ga Hamersley and Transvaal BIFs were deposited in a marine basin that was stratified with respect to Fe^{2+}_{aq} contents (e.g., Klein and Beukes, 1989; Beukes et al., 1990; Morris, 1993). Well-exposed facies changes in the Transvaal Craton are interpreted to record lateral changes in the depth of marine deposition, where Ca–Mg carbonates of the Campbellrand Supergroup that underlie the Kuruman and Griquatown iron formations are interpreted to reflect deposition in shallow waters of low Fe^{2+}_{aq} content, followed by a transgressive marine sequence that involved deposition of iron formations below wave base in Fe^{2+}_{aq}-rich seawater (Beukes, 1984; Beukes et al., 1990). Although such facies changes are not observed in the Hamersley Basin, the close similarity of the 2.5 Ga Hamersley and Transvaal BIFs (Pickard, 2003) suggests that the Transvaal model of an ocean that was vertically stratified in Fe^{2+}_{aq} contents is applicable to the Hamersley Basin. In such a model, ascending Fe^{2+}_{aq}-rich hydrothermal fluids will become oxidized above the chemocline, inducing precipitation of ferric oxide/hydroxides (Fig. 1). Ferric oxide/hydroxides that formed in the upper water column comprise important precursors to minerals such as magnetite that were produced during early diagenesis near the sediment-water interface (e.g., Klein, 2005).

The flow-through box-model equations used by Chu et al. (2006), which were adapted from those in DePaolo (1981), and presented below, allow calculation of the

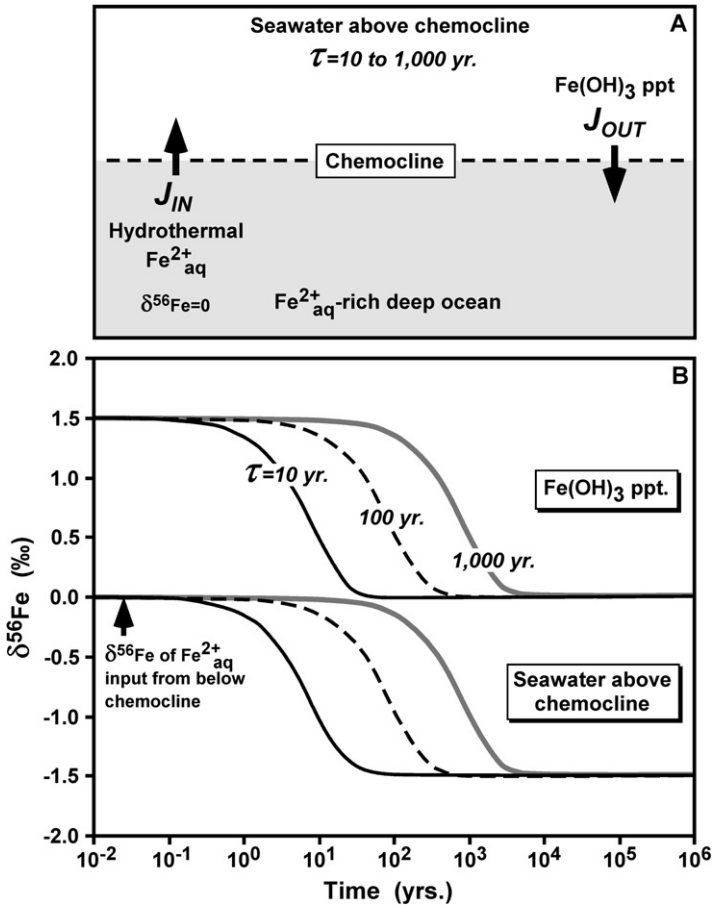

Fig. 7. Flow-through box model illustrating the effects of oxidation and precipitation of Fe^{2+}_{aq} above the chemocline. Schematic (A) illustrates the influx (hydrothermal Fe^{2+}_{aq} from below the chemocline) and outflux (ferric oxide/hydroxide precipitates), which are assumed to be equal, producing steady-state conditions in terms of Fe concentrations above the chemocline. Variations in $\delta^{56}Fe$ values (B) as a function of time, for $Fe(OH)_3$ precipitate and Fe^{2+}_{aq} above the chemocline. Model assumes equilibrium Fe isotope fractionation between Fe^{2+}_{aq} and $Fe(OH)_3$ precipitate is maintained (model is not analogous to Rayleigh fractionation). Calculations demonstrate that if the Fe residence time in seawater above the chemocline is short, the $\delta^{56}Fe$ values of the $Fe(OH)_3$ precipitates will rapidly move toward the $\delta^{56}Fe$ value of the input hydrothermal Fe^{2+}_{aq}; at this point, the $\delta^{56}Fe$ value of $Fe(OH)_3$ precipitates will be independent of the $Fe(OH)_3 - Fe^{2+}_{aq}$ fractionation factor. Although the $\delta^{56}Fe$ values for Fe^{2+}_{aq} above the chemocline will be strongly affected in this model, this reservoir does not affect the $\delta^{56}Fe$ value of Fe delivered to the site of BIF deposition in the deep oceans.

$\delta^{56}Fe$ values of seawater in the Fe^{2+}_{aq}-poor upper water column above the chemocline, as well as the Fe isotope compositions of the ferric oxide/hydroxide precipitates. We will assume steady-state conditions, where the upwelling hydrothermal Fe flux is equal to the outgoing ferric oxide/hydroxide precipitate flux that settles to the Fe^{2+}_{aq}-rich zone beneath the chemocline (Fig. 7A). We define the Fe residence time for seawater above the chemocline as:

$$\tau = M_{SW}/J = M_{SW}/(M_{IN}/t) = M_{SW}/(M_{OUT}/t) \quad (6)$$

where M_{SW} equals the total molar Fe inventory of seawater above the chemocline, J is the Fe flux (moles/time), M_{IN} is the molar Fe concentration of the incoming hydrothermal Fe flux, M_{OUT} is the molar Fe concentration of the outgoing $Fe(OH)_3$ precipitate flux, and t is time. The $\delta^{56}Fe$ values of seawater above the chemocline, using the equations of Chu et al. (2006) and the residence time defined above, are given by:

$$\delta^{56}Fe_{SW} = \delta^{56}Fe_{IN} - \Delta^{56}Fe_{Fe(OH)_3-Fe^{2+}_{aq}}[1 - e^{(-t/\tau)}] \quad (7)$$

where $\delta^{56}Fe_{IN}$ is the Fe isotope composition of the influx and $\Delta^{56}Fe_{Fe(OH)_3-Fe^{2+}_{aq}}$ is the $Fe(OH)_3 - Fe^{2+}_{aq}$ fractionation factor. The instantaneous $\delta^{56}Fe$ value for the $Fe(OH)_3$ precipitate is given by:

$$\delta^{56}Fe_{Fe(OH)_3} = \Delta^{56}Fe_{Fe(OH)_3-Fe^{2+}_{aq}} + \delta^{56}Fe_{SW} \quad (8)$$

We assume $\delta^{56}Fe_{IN} = 0$, based on the discussion above that Archean marine hydrothermal fluids likely had $\delta^{56}Fe$ values that were similar to those of bulk oceanic crust, and the $Fe(OH)_3 - Fe^{2+}_{aq}$ fractionation factor is taken as +1.5‰, based on experimental studies (Beard and Johnson, 2004). Riverine input to seawater above the chemocline under anoxic conditions will likely have $\delta^{56}Fe$ values near the average of igneous rocks, given the fact that weathering under such conditions produces no significant redox change (Yamaguchi et al., 2005). Dissolved riverine input under an oxic atmosphere has variable $\delta^{56}Fe$ values between ~ − 1‰ and +0.2‰ (Fantle and DePaolo, 2004; Bergquist and Boyle, 2006). The dissolved riverine Fe flux into the oceans under an oxic atmosphere, however, is at least an order of magnitude lower than the marine hydrothermal Fe flux (e.g., Stein and Stein, 1995; Berner and Berner, 1996), and so riverine input can be ignored in our model. The atmospheric Fe flux via dust delivery to the oceans will have $\delta^{56}Fe$ values near-zero (Beard et al., 2003b), and so can also be ignored.

The calculations demonstrate that after the residence time is exceeded by approximately a factor of 5, the $\delta^{56}Fe$ value of the ferric oxide/hydroxide precipitates will equal that of the incoming hydrothermal Fe^{2+}_{aq} (Fig. 7B), indicating that the $\delta^{56}Fe$ values of the ferric oxide/hydroxide "rain" will be independent of the $Fe(OH)_3 - Fe^{2+}_{aq}$ fractionation factor once the residence time is significantly exceeded. In terms of BIF genesis, the important conclusion of the calculations illustrated in Fig. 7 lies in the fact that the ferric oxide/hydroxide precipitates which will settle to the site of BIF formation will tend to have $\delta^{56}Fe$ values equal to those of the marine hydrothermal Fe^{2+}_{aq} sources, assuming that essentially complete oxidation and precipitation occurred above the chemocline. Finally, we note that a vertical gradient in Fe residence times may be modeled using multiple boxes, but this does not affect the end result if complete oxidation occurs.

5.4. Iron pathways during magnetite formation

We consider three pathways of magnetite formation during diagenesis: (1) addition of limited quantities of Fe^{2+}_{aq} to the initial ferric oxide/hydroxide precipitates, (2) formation of magnetite in the presence of excess Fe^{2+}_{aq}, and (3) formation of magnetite by DIR. Reduction of the initial ferric oxide/hydroxide precipitates through addition of electrons by sulfide (e.g., Poulton et al., 2004) or abiologic oxidation of organic carbon (e.g., Perry et al., 1973) can be rejected for the Hamersley–Transvaal BIFs. Sulfides are very rare in the magnetite layers, indicating that little sulfide was present. Addition of electrons through abiologic oxidation of organic carbon is unlikely for BIFs that have not been significantly metamorphosed, such as those in the current study, because abiologic reduction of Fe^{3+} coupled to oxidation of organic carbon is not significant, even up to 120 °C (Lovley et al., 1991). Moreover, the $\delta^{13}C$ values for organic carbon in oxide-facies BIFs are generally 10–15‰ higher than those for organic carbon from related shales and iron-poor carbonates (e.g., Beukes et al., 1990), which is opposite of the trend that is predicted for abiologic oxidation of organic carbon accompanied by CO_2 loss (see discussion in Johnson et al., 2003).

5.4.1. Iron addition

Addition of Fe^{2+} to ferric oxide/hydroxide follows common models for magnetite formation in BIFs that involve settling of ferric oxide/hydroxides into Fe^{2+}_{aq}-rich anoxic bottom waters, followed by reaction to form magnetite (Klein, 2005). Addition of just enough Fe^{2+} to ferric oxide/hydroxide to make magnetite may be considered an "Fe^{2+}_{aq} limited" case and would involve simple mixing in the 2:1 Fe^{3+}:Fe^{2+} stoichiometric proportions of magnetite; these relations are shown as the two high-angle lines in Fig. 8 for two $\delta^{56}Fe$ values for the initial ferric oxide/hydroxides. The near-zero peak in $\delta^{56}Fe$ values of magnetite (Fig. 8A) can be produced through addition of Fe^{2+} from seawater ($\delta^{56}Fe = 0$‰) to ferric oxide/hydroxide that also had $\delta^{56}Fe = 0$‰ (Fig. 8). In this model, magnetite that has $\delta^{56}Fe > 0$ would reflect inheritance from ferric oxide/hydroxides that formed through partial oxidation of Fe^{2+}_{aq}. Magnetite that has negative $\delta^{56}Fe$ values, however, requires addition of Fe^{2+}_{aq} that has very low $\delta^{56}Fe$ values, generally between −1.0‰ and −3.0‰ (Fig. 8).

5.4.2. Excess aqueous iron

The isotopic compositions of magnetite that formed in isotopic equilibrium in the presence of excess Fe^{2+}_{aq} will be constrained by the equilibrium magnetite–Fe^{2+}_{aq} fractionation factor, which is shown as the low-angle line in Fig. 8. It is possible that excess Fe^{2+}_{aq} was present, given the water-rich nature of the primary BIF sediment (Trendall and Blockley, 1970), and the fact that siderite is intimately associated with magnetite (e.g., Klein, 2005). Justification for assuming isotopic equilibrium between

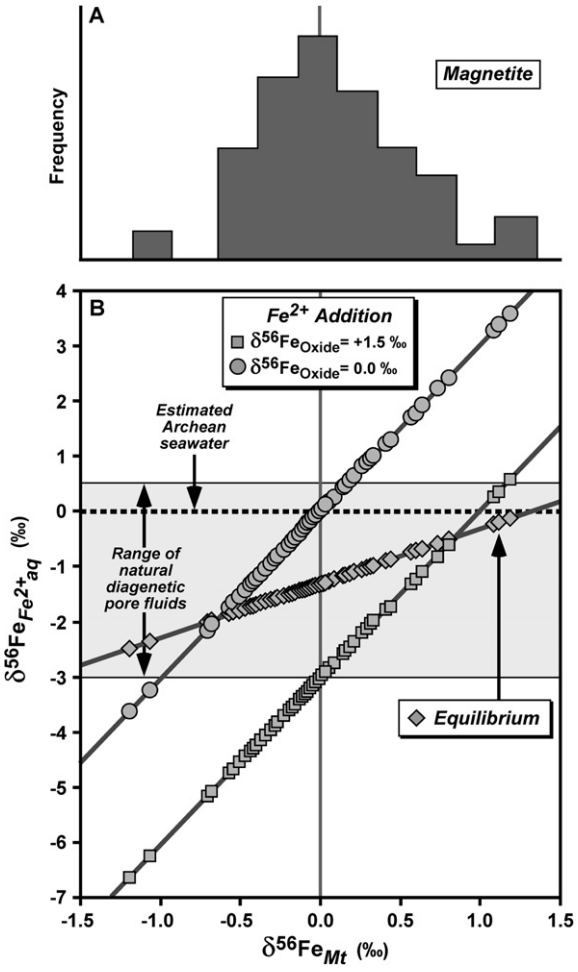

Fig. 8. Comparison of the distribution of Fe isotope compositions for magnetite from the Hamersley–Transvaal BIFs (A) with sources of Fe^{2+}_{aq} (B) that are required to produce the measured $\delta^{56}Fe$ values for magnetite by various pathways. The range in $\delta^{56}Fe$ values for Fe^{2+}_{aq} that is required to produce magnetite through mixing in the stoichiometric 2:1 Fe^{3+}:Fe^{2+} proportions of magnetite ("Fe^{2+} addition") is shown by the high-angle lines (B) for two different $\delta^{56}Fe$ values for the Fe^{3+} component (oxide). Calculated $\delta^{56}Fe$ values for Fe^{2+}_{aq} that would correspond with measured $\delta^{56}Fe$ values for magnetite (squares and circles) are plotted along these mixing lines to illustrate the distribution of data. Assuming a $\delta^{56}Fe$ value of zero for Fe^{2+}, the near-zero to positive $\delta^{56}Fe$ values for magnetite can be produced using Fe^{3+} oxides that had $\delta^{56}Fe = 0$ to +1.5‰; magnetite that has negative $\delta^{56}Fe$ values can only be produced using Fe^{2+} that has negative $\delta^{56}Fe$ values, such as Fe^{2+}_{aq} from natural diagenetic pore fluids where DIR is active (Bergquist and Boyle, 2006; Severmann et al., 2006). The low-angle line shows the range in $\delta^{56}Fe$ values for Fe^{2+}_{aq} that would be in isotopic equilibrium with magnetite of varying $\delta^{56}Fe$ value, using a magnetite–Fe^{2+}_{aq} fractionation factor of −1.3‰ (Johnson et al., 2005); measured data plotted along the equilibrium line are shown in diamonds. If seawater Fe^{2+}_{aq} had $\delta^{56}Fe$ values near zero (see text), only a few of the magnetites that have the highest $\delta^{56}Fe$ values would be in Fe isotope equilibrium with seawater.

Fe^{2+}_{aq} and magnetite comes from experimental work that demonstrates attainment of isotopic equilibrium between Fe^{2+}_{aq} and fine-grained magnetite (<100 nm) within ~2 weeks at room temperature (Johnson et al., 2005). In the case of equilibrium with excess Fe^{2+}_{aq}, however, only magnetite that has the highest $\delta^{56}Fe$ values (~+1.0‰) would be in isotopic equilibrium with seawater Fe^{2+} (Figs. 6 and 8), which seems improbable. If equilibrium with excess Fe^{2+}_{aq} is assumed, the peak in $\delta^{56}Fe$ values for magnetite at $\delta^{56}Fe = 0‰$ would imply equilibrium with Fe^{2+}_{aq} that had a $\delta^{56}Fe$ value of −1.3‰ (Figs. 6 and 8), where the great abundance of magnetite of these compositions suggests a very large Fe^{2+}_{aq} reservoir that has negative $\delta^{56}Fe$ values. Finally, magnetite that has $\delta^{56}Fe < 0‰$ would require exchange with Fe^{2+}_{aq} that had very low $\delta^{56}Fe$ values in the equilibrium model, down to ~ − 2.5‰ (Figs. 6 and 8).

Our preferred model is that $\delta^{56}Fe_{Magnetite} \geqslant 0‰$ reflects a significant inheritance in the isotopic compositions of precursor ferric oxide/hydroxide precipitates, followed by conversion to magnetite through interaction with seawater Fe^{2+}, dissimilatory Fe^{3+} reduction (DIR), or a combination of the two. Although mixing seawater Fe^{2+}_{aq} of $\delta^{56}Fe = 0$ with ferric oxide/hydroxides that had $\delta^{56}Fe = 0$ seems the most likely explanation for the near-zero peak in $\delta^{56}Fe_{Magnetite}$ values, we cannot distinguish this model from complete conversion of ferric oxide/hydroxides to magnetite by DIR under Fe^{2+}_{aq}-limited conditions based on Fe isotopes alone. If complete conversion occurs, the $\delta^{56}Fe$ values of magnetite produced by DIR may be identical to those of the ferric oxide/hydroxide precursors if Fe^{2+}_{aq} contents are relatively low, as demanded by mass-balance constraints (Johnson et al., 2005). Aqueous Fe^{2+} contents are generally low after complete conversion of ferric oxide/hydroxides to magnetite during DIR because the remaining inventory of Fe^{3+} becomes inaccessible to DIR once it is sequestered in magnetite, preventing further reduction (Kostka and Nealson, 1995). Distinguishing between production of magnetite that has near-zero $\delta^{56}Fe$ values through addition of seawater Fe^{2+}_{aq} from complete conversion of ferric oxide/hydroxides by DIR may be possible using O isotopes, given the distinct O isotope compositions that might exist between seawater and the diagenetic pore fluids that would be associated with DIR, particularly pore fluids that might have been associated with silica precipitation.

5.4.3. Role of bacteria in producing low-$\delta^{56}Fe$ magnetite

In all pathways considered, $\delta^{56}Fe_{Magnetite} < 0‰$ requires addition or exchange with very low-$\delta^{56}Fe$ Fe^{2+}_{aq}. That low-$\delta^{56}Fe_{Magnetite}$ values are most common in cores that have the greatest isotopic heterogeneity suggests that the low-$\delta^{56}Fe$ component was a diagenetic fluid. We argue based on extensive experimental studies that coupled electron-Fe atom exchange during partial Fe^{3+} oxide reduction by DIR is the most likely means to produce Fe^{2+}_{aq} that had low $\delta^{56}Fe$ values (Beard et al., 1999, 2003a; Crosby et al., 2005, 2007; Johnson et al., 2005). Low $\delta^{56}Fe$ values have been measured for Fe^{2+}_{aq} in diagenetic pore fluids in modern marine sediments where DIR is active (Bergquist and Boyle, 2006; Severmann et al., 2006). The low $\delta^{56}Fe$ values for Fe^{2+}_{aq} produced by DIR in experiments are generally associated with <10% reduction, and a steady-state condition of partial reduction seems likely to have been sustained by a continual flux of ferric oxide/hydroxide "rain", as well

as organic carbon from photosynthesis in the upper water column, during the entire interval of BIF deposition. We envision a heterogeneous sediment section in which low-δ^{56}Fe Fe^{2+}_{aq} produced by DIR is transported to other sediment sections to explain the entire range in δ^{56}Fe values. This concept is entirely consistent with the fine-scale Fe isotope heterogeneity that is observed in the BIFs (this study) and in modern marine sediments where DIR is active (Severmann et al., 2006). Moreover, the decreasing abundance in $\delta^{56}Fe_{Magnetite}$ values that are most negative, implying a decreasing abundance of the lowest-δ^{56}Fe Fe^{2+}_{aq} (Fig. 8), is exactly what is observed in experiments and natural systems where DIR occurs (Severmann et al., 2006; Crosby et al., 2007), where the lowest Fe^{2+}_{aq} contents produced at small extents of reduction have the lowest δ^{56}Fe values. In this regard, magnetite that has high-δ^{56}Fe values may not necessarily reflect partial oxidation in the upper water column, but may instead reflect the high-δ^{56}Fe oxide component that is produced by DIR (Crosby et al., 2007); resolution of these different interpretations must await further study.

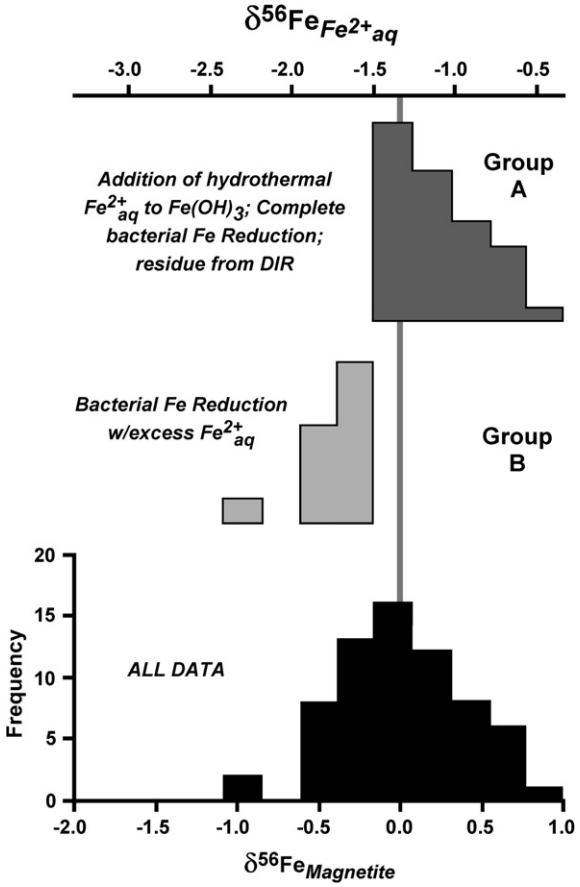

Fig. 9. Histograms of δ^{56}Fe values for magnetite from the Hamersley–Transvaal BIFs, divided by interpretation of magnetite genesis. Magnetite that has $\delta^{56}Fe = 0$ to +1.0‰ is interpreted to have inherited its Fe isotope composition from precursor ferric oxide/hydroxides, followed by conversion to magnetite via interaction with hydrothermal Fe^{2+}_{aq} ($\delta^{56}Fe = 0$), or, possibly, DIR. Magnetite that has negative δ^{56}Fe values requires interaction with low-δ^{56}Fe Fe^{2+}_{aq}, which was most likely produced by DIR.

We summarize our interpretation for the distribution of δ^{56}Fe values for magnetite in Fig. 9. Magnetite that belongs to group A may reflect addition of hydrothermal Fe^{2+}_{aq} to $Fe(OH)_3$ that was produced by complete or near-complete oxidation in the upper water column. Alternatively, these compositions may be produced by complete bacterial Fe(III) reduction. Magnetite that had $\delta^{56}Fe > 0$ may also reflect the oxide residue produced by DIR. Magnetite that has $\delta^{56}Fe < 0$ (group A in Fig. 9) formed by DIR in the presence of excess Fe^{2+}_{aq}, or through addition of low-δ^{56}Fe Fe^{2+}_{aq} that was produced by DIR to precursor ferric oxide/hydroxides.

There are alternative explanations for producing low-δ^{56}Fe aqueous Fe^{2+} other than DIR. Several studies have proposed that sorption of Fe^{2+} to ferric oxide/hydroxides can produce Fe^{2+}_{aq} that has low δ^{56}Fe values, as inferred from measurements of modern groundwater during rapid oxygen-injection experiments (Teutsch et al., 2005), or indirect inference in experiment (Icopini et al., 2004). Extensive oxidation of Fe^{2+}_{aq}, followed by removal of high-δ^{56}Fe oxides, will produce low-δ^{56}Fe values in the remaining Fe^{2+}_{aq} (Bullen et al., 2001). Abiologic dissolution of oxide and silicate minerals by organic ligands has been shown to produce low-δ^{56}Fe aqueous Fe (Brantley et al., 2004; Wiederhold et al., 2006). In none of these processes, however, are large quantities of low-δ^{56}Fe aqueous Fe produced, making them difficult to invoke as an explanation for the large inventory of low-δ^{56}Fe BIFs and shales of Late Archean and Early Proterozoic age (Johnson et al., in press). The quantities of aqueous Fe that have negative δ^{56}Fe values that are produced by sorption, oxidation and precipitation, or abiologic dissolution of oxides or silicates are two to five orders-of-magnitude lower than those produced by DIR (Johnson et al., in press). We conclude, therefore, that at a minimum, DIR is required to explain magnetite that has negative δ^{56}Fe values, and, depending upon the specific iron pathways, virtually the entire inventory of magnetite in the Hamersley–Transvaal BIFs could have been produced through DIR (Fig. 9).

5.5. Iron pathways during siderite formation

The frequency distribution of δ^{56}Fe values for siderite suggests two peaks, one at ~ -0.5‰ and a second at ~0.0‰ (Fig. 10). The peak in δ^{56}Fe values for siderite at −0.5‰ coincides with $\delta^{56}Fe = 0$‰ for Fe^{2+}_{aq}, using the Fe^{2+}_{aq}–siderite fractionation factor from Wiesli et al. (2004) (group A in Fig. 10). This may indicate that many siderites formed in Fe isotope equilibrium with seawater Fe^{2+}, which stands in marked contrast to the conclusions reached for magnetite in the presence of excess Fe^{2+}, where only the few highly positive $\delta^{56}Fe_{Magnetite}$ values could reflect equilibrium with seawater. The secondary peak at $\delta^{56}Fe_{Siderite} = 0.0$‰ would correspond to a δ^{56}Fe value for Fe^{2+}_{aq} of +0.5‰, assuming equilibrium Fe^{2+}_{aq}–siderite fractionation (group B in Fig. 10); this is significantly higher than any estimate of seawater δ^{56}Fe values, which should have been equal to or less than zero, as discussed above. If a Fe^{2+}_{aq}–ankerite fractionation factor is used (Polyakov and Mineev, 2000; Johnson et al., 2005), the calculated δ^{56}Fe

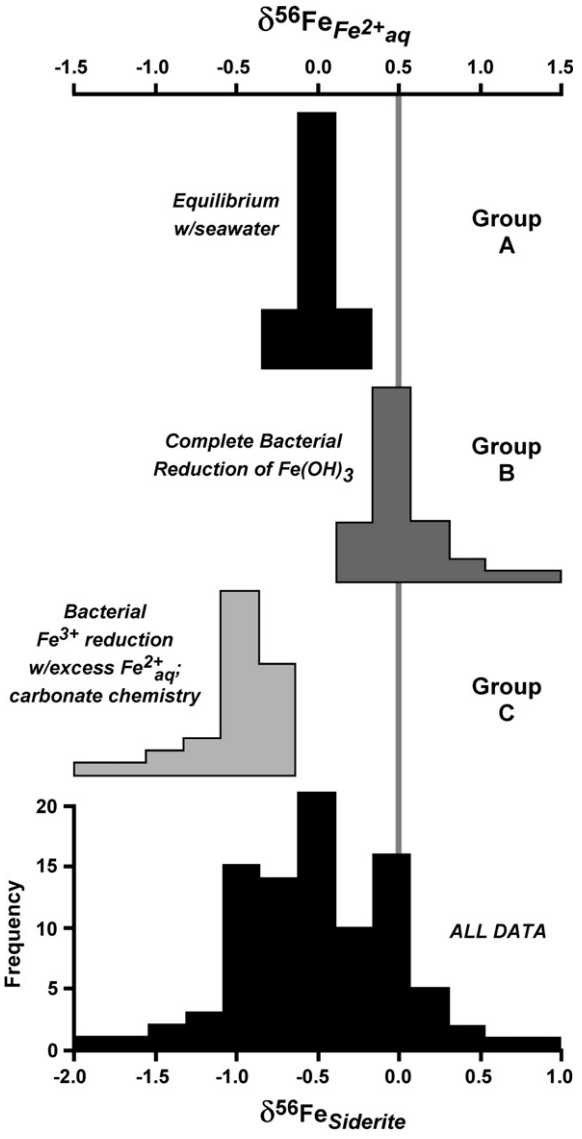

Fig. 10. Histograms of $\delta^{56}Fe$ values for siderite from the Hamersley-Transvaal BIFs, grouped by interpretation of siderite genesis. The main peak about $\delta^{56}Fe_{Siderite} = -0.5‰$ (top) is interpreted to reflect formation in Fe isotope equilibrium with seawater. The secondary peak at $\delta^{56}Fe_{Siderite} = 0‰$ (upper middle) may be explained through inheritance from ferric oxide/hydroxide precursors, followed by complete reduction to siderite by DIR. Siderite that has $\delta^{56}Fe < -0.5‰$ (lower middle) may be explained through isotopic exchange with low-$\delta^{56}Fe$ Fe^{2+}_{aq}, or may reflect the effects of Ca substitution.

values for seawater Fe^{2+}_{aq} will become even higher. Based on these constraints, we interpret the distribution of $\delta^{56}Fe$ values for siderite to reflect three Fe pathways (Fig. 10):

(1) Siderites that belong to the main peak of $\delta^{56}Fe_{Siderite} \sim -0.5‰$ reflect isotopic equilibration with seawater (group A of Fig. 10). This might reflect direct precipitation in the water column or precipitation just beneath the sediment-water interface if Fe^{2+}_{aq} in pore fluids were in isotopic equilibrium with the overlying seawater.

(2) For siderites that belong to the secondary peak at $\delta^{56}Fe_{Siderite} \sim 0‰$, and for $\delta^{56}Fe_{Siderite} > 0‰$ (group B in Fig. 10), the range in Fe isotope compositions seems best explained through inheritance from ferric oxide/hydroxide precursors, followed by complete reduction by DIR. Siderites that have this range in isotopic compositions did not form in equilibrium with seawater. The distribution of $\delta^{56}Fe$ values for this group is similar to that predicted for precursor ferric oxide/hydroxides that were produced by complete or near-complete oxidation, which should have $\delta^{56}Fe \sim 0‰$, but may have a few values where $\delta^{56}Fe > 0$ that reflect partial oxidation. Complete conversion of oxide/hydroxide precursors to siderite would preserve this Fe isotope distribution.

(3) Siderites that have $\delta^{56}Fe$ values significantly less than $-0.5‰$ may be explained through equilibration with excess Fe^{2+}_{aq} that had negative $\delta^{56}Fe$ values (group C in Fig. 10), as might be produced by DIR. Alternatively, these low $\delta^{56}Fe_{Siderite}$ values could reflect the effects of alkaline-earth substitution, given the increase in Fe^{2+}_{aq}–Fe carbonate fractionation upon Ca substitution relative to siderite (Polyakov and Mineev, 2000; Johnson et al., 2005), and hence could have formed in isotopic equilibrium with seawater.

Support for a model where siderite formation reflects variable contributions from biologic and abiologic pathways comes from carbon abundances and isotope compositions. Konhauser et al. (2005) calculated the possible Fe and C fluxes that may have been associated with microbial oxidation and reduction during BIF genesis, and concluded that anaerobic photosynthesis in the upper water column could have supplied the organic carbon and Fe^{3+} fluxes required to produce the measured inventory of magnetite and siderite by DIR. Support for a biological role in siderite formation comes from the fact that siderite in BIFs have $\delta^{13}C$ values that range down to $-15‰$, much lower than the near-zero values of related Ca–Mg carbonates (Fig. 11). Although Becker and Clayton (1972) and Baur et al. (1985) interpreted such low $\delta^{13}C$ values to reflect biological sources of carbon during siderite formation, at the time experimental data for C isotope fractionation during bacterial redox transformations were not yet available.

Recent experimental studies on C isotope fractionation produced by DIR, however (Romanek et al., 2003), indicate that carbonate produced by oxidation of organic carbon via DIR would be expected to produce $\delta^{13}C$ values for carbonate of $\sim -15‰$ to $-25‰$, assuming organic carbon had a $\delta^{13}C$ value of $-20‰$ to $-30‰$ (Fig. 11). Because $\delta^{13}C$ values for Fe-rich carbonates from the 2.5 Ga BIFs of the Transvaal Craton generally decrease with increasing Fe contents (Fig. 11), the range in $\delta^{13}C$ values may be explained as mixtures between seawater carbonate ($\delta^{13}C \sim 0.0‰$) and carbonate that formed via DIR ($\delta^{13}C \sim -15‰$ to $-25‰$). Some scatter in $\delta^{13}C$–Fe content relations is expected in such a model, given the range in carbon-

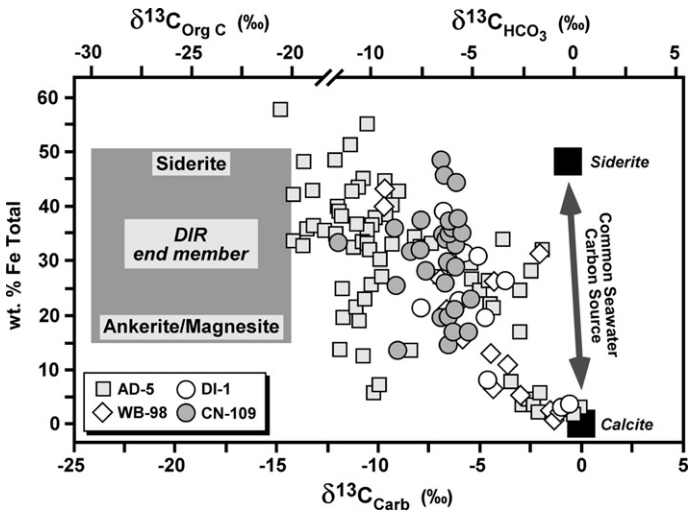

Fig. 11. Variations in $\delta^{13}C$ values for Fe-bearing carbonates from the Kuruman and Griquatown iron formations, Transvaal Craton (South Africa), relative to Fe contents. Carbon isotope compositions and Fe contents from Beukes et al. (1990), Beukes and Klein (1990), and Kaufman (1996). The range in $\delta^{13}C$ values cannot be explained by differences in C isotope fractionations for calcite and siderite (Jimenez-Lopez et al., 2001; Jimenez-Lopez and Romanek, 2004), but are instead interpreted to reflect mixtures between low-Fe carbonates that formed in C isotope equilibrium with seawater carbonate and Fe-rich carbonates that formed by DIR. The range in $\delta^{13}C$ values measured for the Kuruman and Griquatown iron formations overlaps that measured in core DDH-44 for the Dales Gorge member of the Brockman Iron Formation in the Hamersley Basin, Australia (Kaufman et al., 1990), although Fe contents are not available for the Brockman samples and so are not plotted in the figure. Data includes samples from the AD-5 and CN-109 cores that were also analyzed for Fe isotope compositions (Johnson et al., 2003), although the same samples were not analyzed for C and Fe isotope compositions.

ate stoichiometry of Fe-rich carbonates in BIFs, which include compositions that lie along the siderite–magnesite and ankerite–dolomite solid solutions (Klein and Beukes, 1989). This interpretation contrasts with that of Beukes et al. (1990), who argued that the moderately negative $\delta^{13}C$ values for siderite reflected hydrothermal carbon sources. The contrast in $\delta^{13}C$ values for siderite and Ca–Mg carbonates in BIFs cannot be explained by intrinsic differences in fractionation factors, which predict at most ~0.5‰ differences between siderite and calcite at room temperature (Jimenez-Lopez et al., 2001; Jimenez-Lopez and Romanek, 2004). Although C and Fe isotopes have yet to be measured on the same carbonate samples, such an approach would provide a test of this model.

5.6. Late Archean to Early Proterozoic BIF formation: a record of DIR in earth's history?

The important role we infer for DIR in magnetite and siderite genesis in the Hamersley–Transvaal BIFs based on Fe and C isotope data contrasts with the paucity of these minerals in modern coastal marine environments where DIR is active. Several factors may explain this discrepancy: (1) DIR during BIF formation would have been enhanced relative to modern coastal marine systems because delivery of reactive ferric oxide/hydroxides was not diluted by significant clastic input, based on the very low Al contents of oxide- and siderite-facies BIFs (Klein, 2005); (2) siderite production in modern environments is enhanced when bacterial sulfate reduction (BSR) is minor (Coleman, 1993), and low BSR activity at 2.5 Ga (Canfield, 2001) would similarly be expected to favor siderite formation; and (3) magnetite produced by DIR would be more likely to be preserved in 2.5 Ga marine sediments in contrast to modern environments because currently high BSR activity produces sulfide that readily destroys authigenic and detrital magnetite (Karlin and Levi, 1983). It is important to note that although dissolved silica was much higher during BIF formation as compared to today (Siever, 1992), silica does not inhibit Fe(III) reduction rates for DIR that utilizes ferrihydrite as the terminal electron acceptor (Kukkadapu et al., 2004). We conclude that the mineralogical record for DIR, magnetite and siderite, is likely to be well preserved in the Archean record, particularly in rocks that have low clastic contents such as BIFs or other chemical sediments. Low BSR activity would have provided an advantage to DIR because sulfide scavenging of reactive Fe^{3+} would have been minimal. Moreover, low sulfide contents would have allowed preservation of biogenic magnetite and siderite. The low organic carbon contents and the lack of preserved microfossils in BIFs remain a puzzle, but this may reflect efficient conversion to CO_2 during DIR, as well as expulsion of large volumes of fluid during compaction (Trendall and Blockley, 1970) that may have carried away organic matter from the compacting sediment.

The negative $\delta^{56}Fe$ values measured in the 2.5 Ga Hamersley–Transvaal BIFs overlap the range measured for pyrite and black shales of ~2.9 to ~2.4 Ga age (Rouxel et al., 2005; Yamaguchi et al., 2005; Archer and Vance, 2006). Yamaguchi et al. (2005) and Archer and Vance (2006) suggested that the negative $\delta^{56}Fe$ values reflected DIR, whereas Rouxel et al. (2005) preferred extensive oxidation of Fe^{2+}_{aq} to explain the negative $\delta^{56}Fe$ values. Based on correlations among $\delta^{13}C$, $\delta^{34}S$, $\Delta^{33}S$, and $\delta^{56}Fe$ values

for the Late Archean and Early Proterozoic sedimentary rock record, as well as consideration of experimental data from abiological and biological systems, Johnson et al. (in press) argued that a major expansion of DIR occurred between ~3.1 and ~2.4 Ga, where the Hamersley–Transvaal BIF deposition occurred near the end of this expansion.

6. SUMMARY AND CONCLUSIONS

The sensitivity of Fe isotopes to redox changes and extent of reaction provides a direct means for tracing the Fe sources and pathways involved in banded iron formation (BIF) genesis. When coupled to constraints imposed by mass-balance models and experimentally determined isotopic fractionation factors, the Fe isotope data provide the following insights into formation of the extensive 2.5 Ga Hamersley–Transvaal BIFs:

(1) Magnetite did not form in isotopic equilibrium with seawater Fe. Instead, the majority of magnetite, which has near-zero δ^{56}Fe values, directly inherited its Fe isotope compositions from ferric oxide/hydroxide precursors that formed by complete- or near-complete oxidation of hydrothermal Fe^{2+}_{aq}, confirming proposed Fe sources based on REE contents, but also pointing to the presence of a significant oxidant in the upper water column. The oxidant need not have been atmospheric O_2, but could have involved anaerobic photosynthesis (e.g., Widdel et al., 1993). Recent experiments suggest that UV-photo oxidation in natural seawater compositions may be less likely than previously thought (Konhauser et al., 2007). Conversion to magnetite that has near-zero or positive δ^{56}Fe values probably occurred through interaction of precursor ferric oxide/hydroxides with hydrothermal Fe^{2+}_{aq} in the anoxic deep marine environments of BIF deposition; it is also possible that conversion occurred via dissimilatory Fe^{3+} reduction (DIR) by bacteria, which, in the absence of excess Fe^{2+}_{aq}, would produce δ^{56}Fe values for magnetite that match those of the precursor ferric oxide/hydroxides.

(2) The genesis of magnetite that has negative δ^{56}Fe values must have involved low-δ^{56}Fe aqueous Fe^{2+}, regardless of the Fe pathway (limited Fe^{2+} addition; equilibrium with excess Fe^{2+}_{aq}). Production of low-δ^{56}Fe aqueous Fe^{2+} at the site of BIF deposition near the sediment-water interface, which was relatively anoxic, could not have involved extensive ferric oxide/hydroxide precipitation or sorption of Fe^{2+}. Instead we infer a major role for DIR to generate low-δ^{56}Fe Fe^{2+}_{aq} through partial reduction of the ferric oxide/hydroxide "rain" from the upper water column; continuous oxidative processes in the upper water column, which probably involved photosynthesis, supplied the flux of ferric oxide/hydroxides and organic carbon required to sustain a steady-state condition of partial reduction by DIR in the deep marine environments where BIF deposition occurred.

(3) Siderite did not form in Fe isotope equilibrium with magnetite that was deposited in adjacent bands, pointing to distinct Fe pathways for these minerals. Many siderites have δ^{56}Fe values that cluster about −0.5‰, and these likely formed in isotopic equilibrium with seawater Fe; this conclusion stands in marked contrast to the observation that magnetite did not form in Fe isotope equilibrium with seawater. The mass balance for these mildly negative δ^{56}Fe values would have come from the much larger seawater Fe reservoir. A second cluster of Fe isotope compositions for siderite is centered at $\delta^{56}\text{Fe} \sim 0$‰, which cannot reflect isotopic equilibrium with seawater. Instead, these siderites are interpreted to have inherited their Fe isotope compositions from precursor ferric oxide/hydroxides via complete reduction by DIR, and support for a major role for DIR in siderite formation lies in C isotope data. Finally, siderite that has $\delta^{56}\text{Fe} < -0.5$‰ may reflect interaction with Fe^{2+}_{aq} that had low δ^{56}Fe values, or, more likely, the isotopic effects of Ca substitution.

The alternation of Fe-rich and Fe-poor layers in BIFs has been ascribed to seasonal variations (e.g., Trendall and Blockley, 1970), where differences in Fe input may have been caused by variations in hydrothermal input (e.g., Morris, 1993) or differences in ferric oxide/hydroxide fluxes from the upper water column as a function of seasonal variations in photosynthesis (e.g., Cloud, 1973). The major role inferred for DIR in genesis of the 2.5 Ga Hamersley–Transvaal BIFs suggests that variations in the ferric oxide/hydroxide flux to the deep ocean may be the primary controlling factor for banding, at least in the Hamersley–Transvaal BIFs. Several factors may have promoted DIR. Juxtaposition of oxidized and reduced marine environments provided a redox contrast that simultaneously supplied large quantities of ferric oxide/hydroxides and extensive anaerobic environments to support DIR. The evidence that oxidation was extensive in the upper water column, as indicated by the histogram peaks about $\delta^{56}\text{Fe}_{\text{Magnetite}}$ and $\delta^{56}\text{Fe}_{\text{Siderite}} \sim 0$‰ that is interpreted to reflect inheritance from ferric oxide/hydroxide precipitates, is important, because without large quantities of Fe^{3+}, DIR could not occur. The very low clastic sediment input, as well as low rates of bacterial sulfate reduction, at least locally, enhanced conditions required to support DIR and preserved magnetite and siderite products. When compared to earlier BIFs, such as the 3.8 Ga sequences of the Isua Supracrustal Belt, Greenland, the basic components of oxidation and large quantities of Fe^{2+}_{aq} also existed. In contrast to the Fe isotope compositions of the 2.5 Ga BIFs, however, the 3.8 Ga BIFs have δ^{56}Fe values that are almost entirely positive, ranging up to +2.2‰ (Dauphas et al., 2004, 2007; Whitehouse and Fedo, 2007). This is a first-order observation in the temporal Fe isotope record of BIFs, which must indicate very different formation pathways at 2.5 and 3.8 Ga. The generally positive δ^{56}Fe values of the older sequences may reflect lower oxidant abundances, where ferric oxide/hydroxide precursors to magnetite formed through partial oxidation, perhaps less than 10%.

In turn, limited supplies of Fe^{3+} and organic carbon at 3.8 Ga would limit DIR as a major component in Fe cycling. Younger BIFs, such as the 1.9 Ga Biwabik Iron Formation (Frost et al., 2006; Valaas-Hyslop et al., in press), so far appear to have generally zero to positive $\delta^{56}Fe$ values, which may be explained by a contraction in the extent of DIR as oceanic sulfide contents increased, which titrated reactive Fe^{3+} from the oceans (Johnson et al., in press). The voluminous 2.5 Ga Hamersley–Transvaal BIFs, therefore, may represent a time of maximum expansion of DIR on Earth.

ACKNOWLEDGMENTS

This work was supported by NSF Grant EAR-0525417 to CMJ, BLB, and EER. We thank Julie O'Leary, Ashley Hubbard, Aaron Shultis, and Rene Wiesli for assistance in the Fe isotope analyses. We thank Derek Vance, Edwin Schauble, and Kurt Konhauser for valuable reviews, and Jim McManus for editorial handling.

REFERENCES

Albarede F. and Beard B. (2004) Analytical methods for non-traditional isotopes. In *Geochemistry of Non-Traditional Stable Isotopes, Rev. in Mineralogy and Geochemistry*, vol. 55 (eds. C. M. Johnson, B. L. Beard and F. Albarède). Mineralogical Society of America and Geochemical Society, Washington DC, pp. 113–152.

Anbar A. D. and Rouxel O. (2007) Metal Stable Isotopes in Paleoceanography. *Annu. Rev. Earth Planet. Sci.* **35**, 717–746.

Archer C. and Vance D. (2006) Coupled Fe and S isotope evidence for Archean microbial Fe(III) and sulfate reduction. *Geology* **34**(3), 153–156.

Balci N., Bullen T. D., Witte-Lien K., Shanks W. C., Motelica M. and Mandernack K. W. (2006) Iron isotope fractionation during microbially stimulated Fe(II) oxidation and Fe(III) precipitation. *Geochim. Cosmochim. Acta* **70**(3), 622–639.

Bau M., Hohndorf A., Dulski P. and Beukes N. J. (1997) Sources of rare-earth elements and iron in paleoproterozoic iron-formations from the Transvaal Supergroup, South Africa: evidence from neodymium isotopes. *J. Geol.* **105**(1), 121–129.

Bau M. and Möller P. (1993) Rare earth element systematics of the chemically precipitated component in Early Precambrian iron-formations and the evolution of the terrestrial atmosphere–hydrosphere–lithosphere system. *Geochim. Cosmochim. Acta* **57**, 2239–2249.

Baur M. E., Hayes J. M., Studley S. A. and Walter M. R. (1985) Millimeter-scale variations of stable isotope abundances in carbonates from banded iron-formations in the Hamersley Group of Western-Australia. *Econ. Geol.* **80**(2), 270–282.

Beard B. L. and Johnson C. M. (2004) Fe isotope variations in the modern and ancient earth and other planetary bodies. In *Geochemistry of Non-Traditional Stable Isotopes, Rev. in Mineralogy and Geochemistry*, vol. 55 (eds. C. M. Johnson, B. L. Beard and F. Albarède). Mineralogical Society of America and Geochemical Society, Washington DC, pp. 319–357.

Beard B. L. and Johnson C. M. (2006) Comment on "Heavy iron isotope composition of granites determined by high resolution MC-ICP-MS", by F. Poltrasson and R. Freydier [Chem. Geol. 222, 132–147]. *Chem. Geol.* 235, pp. 201–204.

Beard B. L., Johnson C. M., Cox L., Sun H., Nealson K. H. and Aguilar C. (1999) Iron isotope biosignatures. *Science* **285**(5435), 1889–1892.

Beard B. L., Johnson C. M., Skulan J. L., Nealson K. H., Cox L. and Sun H. (2003a) Application of Fe isotopes to tracing the geochemical and biological cycling of Fe. *Chem. Geol.* **195**(1–4), 87–117.

Beard B. L., Johnson C. M., Von Damm K. L. and Poulson R. L. (2003b) Iron isotope constraints on Fe cycling and mass balance in oxygenated Earth oceans. *Geology* **31**(7), 629–632.

Becker R. H. and Clayton R. N. (1972) Carbon isotopic evidence for the origin of a banded iron-formation in Western Australia. *Geochim. Cosmochim. Acta* **36**(5), 577–595.

Bergquist B. A. and Boyle E. A. (2006) Iron isotopes in the Amazon River system: weathering and transport signatures. *Earth Planet. Sci. Lett.* **248**, 54–68.

Berner E. K. and Berner R. A. (1996) *Global Environment: Water, Air, and Geochemical Cycles*. Prentice Hall.

Beukes N. J. (1984) Sedimentology of the Kuruman and Griquatown iron-formations, Transvaal Supergroup, Griqualand West, South-Africa. *Precamb. Res.* **24**(1), 47–84.

Beukes N. J. and Klein C. (1990) Geochemistry and sedimentology of a facies transition—from microbanded to granular iron-formation—in the early proterozoic Transvaal Supergroup, South-Africa. *Precamb. Res.* **47**(1–2), 99–139.

Beukes N. J., Klein C., Kaufman A. J. and Hayes J. M. (1990) Carbonate petrography, kerogen distribution, and carbon and oxygen isotope variations in an early proterozoic transition from limestone to iron-formation deposition, Transvaal Supergroup. *S. Afr. Econ. Geol.* **85**(4), 663–690.

Brantley S. L., Liermann L. J., Guynn R. L., Anbar A., Icopini G. A. and Barling J. (2004) Fe isotopic fractionation during mineral dissolution with and without bacteria. *Geochim. Cosmochim. Acta* **68**(15), 3189–3204.

Bullen T. D., White A. F., Childs C. W., Vivit D. V. and Schulz M. S. (2001) Demonstration of significant abiotic iron isotope fractionation in nature. *Geology* **29**(8), 699–702.

Canfield D. E. (2001) Biogeochemistry of sulfur isotopes. In *Stable Isotope Geochemistry, Rev. in Mineralogy and Geochemistry*, vol. 43 (eds. J. W. Valley and D. R. Cole). Mineralogical Society of America and Geochemical Society, Washington DC, pp. 607–636.

Canfield D. E. (2005) The early history of atmospheric oxygen: homage to Robert Garrels. *Annu. Rev. Earth Planet. Sci.* **33**, 1–36.

Canfield D. E. and Raiswell R. (1999) The evolution of the sulfur cycle. *Am. J. Sci.* **299**, 697–723.

Chu N. C., Johnson C. M., Beard B. L., German C. R., Nesbitt R. W., Frank M., Bohn M., Kubik P. W., Usui A. and Graham I. (2006) Evidence for hydrothermal venting in Fe isotope compositions of the deep Pacific Ocean through time. *Earth Planet. Sci. Lett.* **245**(1–2), 202–217.

Cloud P. (1968) Atmospheric and hydrospheric evolution on the primitive earth. *Science* **160**, 729–736.

Cloud P. (1973) Paleoecological significance of banded iron-formation. *Econ. Geol.* **68**(7), 1135–1143.

Coleman M. L. (1993) Microbial processes—controls on the shape and composition of carbonate concretions. *Mar. Geol.* **113**(1–2), 127–140.

Croal L. R., Johnson C. M., Beard B. L. and Newman D. K. (2004) Iron isotope fractionation by Fe(II)-oxidizing photoautotrophic bacteria. *Geochim. Cosmochim. Acta* **68**(6), 1227–1242.

Crosby H. A., Johnson C. M., Roden E. E. and Beard B. L. (2005) Coupled Fe(II)–Fe(III) electron and atom exchange as a mechanism for Fe isotope fractionation during dissimilatory iron oxide reduction. *Environ. Sci. Technol.* **39**(17), 6698–6704.

Crosby H. A., Roden E. E., Johnson C. M. and Beard B. L. (2007) The mechanisms of iron isotope fractionation produced during

dissimilatory Fe(III) reduction by Shewanella putrefaciens and Geobacter sulfurreducens. *Geobiol.* **5**(2), 169–189.

Dauphas N., Van Zuilen M., Busigny V., Lepland A., Wadhwa M. and Janney P. E. (2007) Iron isotope, major and trace element characterization of early Archean supracrustal rocks from SW Greenland: protolith identification and metamorphic overprint. *Geochim. Cosmochim. Acta* **71**, 4745–4770.

Dauphas N., van Zuilen M., Wadhwa M., Davic A. M., Marty B. and Janney P. E. (2004) Clues from Fe isotope variaitons on the origin of Early Archean BIFs from Greenland. *Science* **306**, 2077–2080.

DePaolo D. J. (1981) Trace element and isotopic effects of combined wallrock assimilation and fractional crystallization. *Earth Planet. Sci. Lett.* **53**(2), 189–202.

Ewers W. E. (1983) Chemical factors in the deposition and diagenesis of banded iron-formation. In *Iron-Formations: Facts and Problems* (eds. A. F. Trendall and R. C. Morris). Elsevier, pp. 491–512.

Ewers W. E. and Morris R. C. (1981) Studies of the Dales-Gorge-Member of the Brockman-Iron-Formation, Western Australia. *Econ. Geol.* **76**(7), 1929–1953.

Fantle M. S. and DePaolo D. J. (2004) Iron isotopic fractionation during continental weathering. *Earth Planet. Sci. Lett.* **228**, 547–562.

Frost C. D., Von Blanckenburg F., Schoenberg R., Frost B. R. and Swapp S. M. (2006) Preservation of Fe isotope heterogeneities during diagenesis and metamorphism of banded iron formation. *Contrib. Mineral. Petrol.* **153**, 211–235.

Icopini G. A., Anbar A. D., Ruebush S. S., Tien M. and Brantley S. L. (2004) Iron isotope fractionation during microbial reduction of iron: The importance of adsorption. *Geology* **32**(3), 205–208.

Jimenez-Lopez C., Caballero E., Huertas F. J. and Romanek C. S. (2001) Chemical, mineralogical and isotope behavior, and phase transformation during the precipitation of calcium carbonate minerals from intermediate ionic solution at 25 °C. *Geochim. Cosmochim. Acta* **65**, 3219–3231.

Jimenez-Lopez C. and Romanek C. S. (2004) Precipitation kinetics and carbon isotope partitioning of inorganic siderite at 25 °C and 1 atm. *Geochim. Cosmochim. Acta* **68**, 557–571.

Johnson C. M., Beard B. L., Beukes N. J., Klein C. and O'Leary J. M. (2003) Ancient geochemical cycling in the Earth as inferred from Fe isotope studies of banded iron formations from the Transvaal Craton. *Contrib. Mineral. Petrol.* **144**(5), 523–547.

Johnson C. M., Beard B. L. and Roden E. E. (in press) The iron isotope fingerprints of redox and biogeochemical cycling in the modern and ancient Earth. *Annu. Rev. Earth Planet. Sci.*

Johnson C. M., Roden E. E., Welch S. A. and Beard B. L. (2005) Experimental constraints on Fe isotope fractionation during magnetite and Fe carbonate formation coupled to dissimilatory hydrous ferric oxide reduction. *Geochim. Cosmochim. Acta* **69**(4), 963–993.

Kappler A., Pasquero C., Konhauser K. O. and Newman D. K. (2005) Deposition of banded iron formations by anoxygenic phototrophic Fe(II)-oxidizing bacteria. *Geology* **33**(11), 865–868.

Karlin R. and Levi S. (1983) Diagenesis of magnetic minerals in recent hemipelagic sediments. *Nature* **303**(5915), 327–330.

Kaufman A. J. (1996) Geochemical and mineralogic effects of contact metamorphism on banded iron-formation: an example from the Transvaal Basin, South Africa. *Precamb. Res.* **79**, 171–194.

Kaufman A. J., Hayes J. M. and Klein C. (1990) Primary and diagenetic controls of isotopic compositions of iron-formation carbonates. *Geochim. Cosmochim. Acta* **54**(12), 3461–3473.

Klein C. (2005) Some Precambrian banded iron-formations (BIFs) from around the world: their age, geologic setting, mineralogy, metamorphism, geochemistry, and origin. *Am. Mineral.* **90**(10), 1473–1499.

Klein C. and Beukes N. J. (1989) Geochemistry and sedimentology of a facies transition from limestone to iron-formation deposition in the early proterozoic Transvaal Supergroup, South-Africa. *Econ. Geol.* **84**(7), 1733–1774.

Klein C. and Beukes N. J. (1992) Time distribution, stratigraphy, sedimentologic setting, and geochemistry of Precambrian iron-formations. In *The Proterozoic Biosphere: A Multidisciplinary Study* (eds. J. W. Schopf and C. Klein). Cambridge University Press, pp. 139–146.

Knoll A. H. (2003) The geological consequences of evolution. *Geobiology* **1**, 3–14.

Konhauser K. O., Amskold L., Lalonde S. V., Posth N. R., Kappler A. and Anbar A. (2007) Decoupling photochemical Fe(II) oxidation from shallow-water BIF deposition. *Earth Planet. Sci. Lett.* **258**, 87–100.

Konhauser K. O., Hamade T., Raiswell R., Morris R. C., Ferris F. G., Southam G. and Canfield D. E. (2002) Could bacteria have formed the Precambrian banded iron formations? *Geology* **30**(12), 1079–1082.

Konhauser K. O., Newman D. K. and Kappler A. (2005) The potential significance of microbial Fe(III) reduction during deposition of Precambrian banded iron formations. *Geobiology* **3**, 167–177.

Kostka J. E. and Nealson K. H. (1995) Dissolution and reduction of magnetite by bacteria. *Environ. Sci. Technol.* **29**, 2535–2540.

Kukkadapu R. K., Zachara J. M., Fredrickson J. K. and Kennedy D. W. (2004) Biotransformation of two-line silica-ferrihydrite by a dissimilatory Fe(III)-reducing bacterium: formation of carbonate green rust in the presence of phosphate. *Geochim. Cosmochim. Acta* **68**(13), 2799–2814.

Lovley D. R., Phillips E. J. P. and Lonergan D. J. (1991) Enzymatic versus nonenzymatic mechanisms for Fe(III) reduction in aquatic sediments. *Environ. Sci. Technol.* **25**(6), 1062–1067.

Lovley D. R., Stolz J. F., Nord G. L. and Phillips E. J. P. (1987) Anaerobic production of magnetite by a dissimilatory iron-reducing microorganism. *Nature* **330**(6145), 252–254.

Miyano T. and Beukes N. J. (1984) Phase relations of stilpnomelane, ferri-annite, and riebeckite in very low grade metamorphosed iron formations. *Trans. Geol. Soc. S. Afr.* **87**, 111–124.

Morris R. C. (1993) Genetic modeling for banded iron-formation of the Hamersley Group, Pilbara Craton, Western-Australia. *Precamb. Res.* **60**(1-4), 243–286.

Nealson K. H. and Myers C. R. (1990) Iron reduction by bacteria: a potential role in the genesis of banded iron formations. *Am. J. Sci.* **290A**, 35–45.

Perry E. C., Tan F. C. and Morey G. B. (1973) Geology and Stable Isotope Geochemistry of Biwabik Iron Formation, Northern Minnesota. *Econ. Geol.* **68**(7), 1110–1125.

Pickard A. L. (2003) SHRIMP U–Pb zircon ages for the Palaeoproterozoic Kuruman Iron Formation, Northern Cape Province, South Africa: evidence for simultaneous BIF deposition on Kaapvaal and Pilbara Cratons. *Precamb. Res.* **125**(3-4), 275–315.

Poitrasson F., Halliday A. N., Lee D. C., Levasseur S. and Teutsch N. (2004) Iron isotope differences between Earth, Moon, Mars and Vesta as possible records of contrasted accretion mechanisms. *Earth Planet. Sci. Lett.* **223**(3–4), 253–266.

Polyakov V. B., Clayton R. A., Horita J. and Mineev S. D. (2007) Equilibrium iron isotope fractionation factors of minerals: reevaluation from the data of nuclear inelastic resonant X-ray scattering and Mössbauer spectroscopy. *Geochim. Cosmochim. Acta* **71**, 3833–3846.

Polyakov V. B. and Mineev S. D. (2000) The use of Mössbauer spectroscopy in stable isotope geochemistry. *Geochim. Cosmochim. Acta* **64**, 849–865.

Poulton S. W., Krom M. D. and Raiswell R. (2004) A revised scheme for the reactivity of iron (oxyhdr)oxide minerals towards dissolved sulfide. *Geochim. Cosmochim. Acta* **68**, 3703–3715.

Romanek C. S., Zhang C. L., Li Y., Horita J., Vali H., Cole D. R. and Phelps T. J. (2003) Carbon and hydrogen isotope fractionations associated with dissimilatory iron-reducing bacteria. *Chem. Geol.* **195**(1–4), 5–16.

Rouxel O., Dobbek N., Ludden J. and Fouquet Y. (2003) Iron isotope fractionation during oceanic crust alteration. *Chem. Geol.* **202**(1–2), 155–182.

Rouxel O. J., Bekker A. and Edwards K. J. (2005) Iron isotope constraints on the Archean and Paleoproterozoic ocean redox state. *Science* **307**(5712), 1088–1091.

Rue E. L. and Bruland K. W. (1995) Complexation of iron(III) by natural organic ligands in the Central North Pacific as determined by a new competitive ligand equilibration/adsorptive cathodic stripping voltammetric method. *Mar. Chem.* **50**, 117–138.

Schauble E. A., Rossman G. R. and Taylor H. P. (2001) Theoretical estimates of equilibrium Fe-isotope fractionations from vibrational spectroscopy. *Geochim. Cosmochim. Acta* **65**(15), 2487–2497.

Severmann S., Johnson C. M., Beard B. L., German C. R., Edmonds H. N., Chiba H. and Green D. R. H. (2004) The effect of plume processes on the Fe isotope composition of hydrothermally derived Fe in the deep ocean as inferred from the Rainbow vent site, Mid-Atlantic Ridge, 36 degrees 14′N. *Earth Planet. Sci. Lett* **225**(1–2), 63–76.

Severmann S., Johnson C. M., Beard B. L. and McManus J. (2006) The effect of early diagenesis on the Fe isotope compositions of porewaters and authigenic minerals in continental margin sediments. *Geochim. Cosmochim. Acta* **70**(8), 2006–2022.

Siever R. (1992) The silica cycle in the Precambrian. *Geochim. Cosmochim. Acta* **56**(8), 3265–3272.

Simonson B. M. (2003) Origin and evolution of large Precambrian iron formations. *Geol. Soc. Am. Spec. Pap.* **370**, 231–244.

Staton S. J. R., Amskold L., Gordon G., Anbar A. D. and Konhauser K. O. (2006) Iron isotope fractionation during photo-oxidation of aqueous ferrous iron. In *Astrobiology Science Conference*.

Stein C. A. and Stein S. (1995) Heat flow and hydrothermal circulation. In *Seafloor Hydrothermal Systems—Physical, Chemical, Biological and Geological Interactions*, vol. 91 (eds. S. E. Humphris, R. A. Zierenberg, L. S. Mullineaux and R. E. Thompson). American Geophysical Union, pp. 425–445.

Sumner D. Y. (1997) Carbonate precipitation and oxygen stratification in Late Archean seawater as deduced from facies and stratigraphy of the Gamohaan and Frisco Formations, Transvaal Supergroup. *S. Afr. Am. J. Sci.* **297**, 455–487.

Teutsch N., von Gunten U., Porcelli D., Cirpka O. A. and Halliday A. N. (2005) Adsorption as a cause for iron isotope fractionation in reduced groundwater. *Geochim. Cosmochim. Acta* **69**(17), 4175–4185.

Trendall A. F. (2002) The significance of iron-formation in the Precambrian stratigraphic record. In *Precambrian Sedimentary Environments: A Modern Approach to Depositional Systems*, vol. 44 (eds. W. Altermann and P. L. Corcorane). International Association of Sedimentologists Special Publication, pp. 33–66.

Trendall A. F. and Blockley J. G. (1970) The iron formations of the Precambrian Hamersley Group, Western Australia. *Bull. Geol. Surv. W. Aust.* **119**, 1–366.

Trendall A. F., Compston W., Nelson D. R., De Laeter J. R. and Bennett V. C. (2004) SHRIMP zircon ages constraining the depositional chronology of the Hamersley Group, Western Australia. *Aust. J. Earth Sci.* **51**(5), 621–644.

Valaas-Hyslop E., Valley J. W., Johnson C. M. and Beard B. L. (in press) The effects of metamorphism on O and Fe isotope compositions in the Biwabik iron-formation, northern Minnesota. *Contrib. Mineral. Petrol.*

Whitehouse M. J. and Fedo C. M. (2007) Microscale heterogeneity of Fe isotopes in >3.71 Ga banded iron formation from the Isua Greenstone Belt, southwest Greenland. *Geology* **35**, 719–722.

Widdel F., Schnell S., Heising S., Ehrenreich A., Assmus B. and Schink B. (1993) Ferrous iron oxidation by anoxygenic phototrophic bacteria. *Nature* **362**(6423), 834–836.

Wiederhold J. G., Kraemer S. M., Teutsch N., Borer P. M., Halliday A. N. and Kretzschmar R. (2006) Iron isotope fractionation during proton-promoted, ligand-controlled, and reductive dissolution of goethite. *Environ. Sci. Technol.* **40**(12), 3787–3793.

Wiesli R. A., Beard B. L. and Johnson C. M. (2004) Experimental determination of Fe isotope fractionation between aqueous Fe(II), siderite and ''green rust'' in abiotic systems. *Chem. Geol.* **211**(3–4), 343–362.

Yamaguchi K. E., Johnson C. M., Beard B. L. and Ohmoto H. (2005) Biogeochemical cycling of iron in the Archean-Paleoproterozoic Earth: constraints from iron isotope variations in sedimentary rocks from the Kaapvaal and Pilbara Cratons. *Chem. Geol.* **218**(1–2), 135–169.

Associate editor: James McManus